11-1-2019

Near-Resonance In A System Of Sub-Neptunes From TESS

S. N. Quinn

J. C. Becker

J. E. Rodriguez

S. Hadden

C. X. Huang

See next page for additional authors

Recommended Citation

S. N. Quinn, J. C. Becker, J. E. Rodriguez, S. Hadden, C. X. Huang, T. D. Morton, F. C. Adams, D. Armstrong, J. D. Eastman, J. Homer, S. R. Kane, J. J. Lissauer, J. D. Twicken, A. Vanderburg, R. Wittenmyer, G. R. Ricker, R. K. Vanderspek, D. W. Latham, S. Seager, J. N. Winn, J. M. Jenkins, E. Agol, K. Barkaoui, C. A. Beichman, F. Bouchy, L. G. Bouma, A. Burdanov, J. Campbell, R. Carlino, S. M. Cartwright, D. Charbonneau, J. L. Christiansen, D. Ciardi, K. A. Collins, K. I. Collins, D. M. Conti, I. J. M. Crossfield, T. Daylan, J. Dittmann, J. Doty, D. Dragomir, E. Ducrot, M. Gillon, A. Glidden, R. F. Goeke, E. J. Gonzales, K. G. Hełminiak, E. P. Horch, S. B. Howell, E. Jehin, Eric L.N. Jensen, J. F. Kielkopf, M. H. Kristiansen, N. Law, A. W. Mann, M. Marmier, R. A. Matson, E. Matthews, T. Mazeh, M. Mori, F. Murgas, C. Murray, N. Narita, L. D. Nielsen, G. Ottoni, E. Palle, R. Pawłaszek, F. Pepe, J. Pitogo de Leon, F. J. Pozuelos, H. M. Relles, J. E. Schlieder, D. Sebastian, D. Ségransan, A. Shporer, K. G. Stassun, M. Tamura, S. Udry, I. Waite, J. G. Winters, and C. Ziegler. (2019). "Near-Resonance In A System Of Sub-Neptunes From TESS". *Astronomical Journal*. Volume 158, Issue 5. DOI: 10.3847/1538-3881/ab3f2b
https://works.swarthmore.edu/fac-physics/372

Authors

S. N. Quinn, J. C. Becker, J. E. Rodriguez, S. Hadden, C. X. Huang, T. D. Morton, F. C. Adams, D. Armstrong, J. D. Eastman, J. Homer, S. R. Kane, J. J. Lissauer, J. D. Twicken, A. Vanderburg, R. Wittenmyer, G. R. Ricker, R. K. Vanderspek, D. W. Latham, S. Seager, J. N. Winn, J. M. Jenkins, E. Agol, K. Barkaoui, C. A. Beichman, F. Bouchy, L. G. Bouma, A. Burdanov, J. Campbell, R. Carlino, S. M. Cartwright, D. Charbonneau, J. L. Christiansen, D. Ciardi, K. A. Collins, K. I. Collins, D. M. Conti, I. J. M. Crossfield, T. Daylan, J. Dittmann, J. Doty, D. Dragomir, E. Ducrot, M. Gillon, A. Glidden, R. F. Goeke, E. J. Gonzales, K. G. Hełminiak, E. P. Horch, S. B. Howell, E. Jehin, Eric L.N. Jensen, J. F. Kielkopf, M. H. Kristiansen, N. Law, A. W. Mann, M. Marmier, R. A. Matson, E. Matthews, T. Mazeh, M. Mori, F. Murgas, C. Murray, N. Narita, L. D. Nielsen, G. Ottoni, E. Palle, R. Pawłaszek, F. Pepe, J. Pitogo de Leon, F. J. Pozuelos, H. M. Relles, J. E. Schlieder, D. Sebastian, D. Ségransan, A. Shporer, K. G. Stassun, M. Tamura, S. Udry, I. Waite, J. G. Winters, and C. Ziegler

The Astronomical Journal, 158:177 (16pp), 2019 November https://doi.org/10.3847/1538-3881/ab3f2b

Near-resonance in a System of Sub-Neptunes from *TESS*

Samuel N. Quinn[1], Juliette C. Becker[2], Joseph E. Rodriguez[1], Sam Hadden[1], Chelsea X. Huang[3,45], Timothy D. Morton[4], Fred C. Adams[2], David Armstrong[5,6], Jason D. Eastman[1], Jonathan Horner[7], Stephen R. Kane[8], Jack J. Lissauer[9], Joseph D. Twicken[10], Andrew Vanderburg[11,46], Rob Wittenmyer[7], George R. Ricker[3], Roland K. Vanderspek[3], David W. Latham[1], Sara Seager[3,12,13], Joshua N. Winn[14], Jon M. Jenkins[9], Eric Agol[15], Khalid Barkaoui[16,17], Charles A. Beichman[18], François Bouchy[19], L. G. Bouma[14], Artem Burdanov[20], Jennifer Campbell[47], Roberto Carlino[21], Scott M. Cartwright[22], David Charbonneau[1], Jessie L. Christiansen[18], David Ciardi[18], Karen A. Collins[1], Kevin I. Collins[23], Dennis M. Conti[24], Ian J. M. Crossfield[3], Tansu Daylan[3,48], Jason Dittmann[3], John Doty[25], Diana Dragomir[3,49], Elsa Ducrot[17], Michael Gillon[17], Ana Glidden[3,12], Robert F. Goeke[3], Erica J. Gonzales[26,50], Krzysztof G. Hełminiak[27], Elliott P. Horch[28], Steve B. Howell[9], Emmanuel Jehin[20], Eric L. N. Jensen[29], John F. Kielkopf[30], Martti H. Kristiansen[31,32], Nicholas Law[33], Andrew W. Mann[33], Maxime Marmier[19], Rachel A. Matson[9], Elisabeth Matthews[3], Tsevi Mazeh[34], Mayuko Mori[35], Felipe Murgas[36,37], Catriona Murray[38], Norio Narita[35,36,39,40,41], Louise D. Nielsen[19], Gaël Ottoni[19], Enric Palle[36,37], Rafał Pawłaszek[27], Francesco Pepe[19], Jerome Pitogo de Leon[35], Francisco J. Pozuelos[17,20], Howard M. Relles[1], Joshua E. Schlieder[42], Daniel Sebastian[17], Damien Ségransan[19], Avi Shporer[3], Keivan G. Stassun[23,43], Motohide Tamura[35,40,41], Stéphane Udry[19], Ian Waite[7], Jennifer G. Winters[1], and Carl Ziegler[44]

[1] Center for Astrophysics, Harvard & Smithsonian, 60 Garden Street, Cambridge, MA 02138, USA; squinn@cfa.harvard.edu
[2] Astronomy Department, University of Michigan, 1085 S University Avenue, Ann Arbor, MI 48109, USA
[3] Department of Physics and Kavli Institute for Astrophysics and Space Research, Massachusetts Institute of Technology, Cambridge, MA 02139, USA
[4] Department of Astronomy, University of Florida, 211 Bryant Space Science Center, Gainesville, FL 32611, USA
[5] Deptartment of Physics, University of Warwick, Gibbet Hill Road, Coventry CV4 7AL, UK
[6] Centre for Exoplanets and Habitability, University of Warwick, Gibbet Hill Road, Coventry CV4 7AL, UK
[7] Centre for Astrophysics, University of Southern Queensland, West Street, Toowoomba, QLD 4350, Australia
[8] Department of Earth Sciences, University of California, Riverside, CA 92521, USA
[9] NASA Ames Research Center, Moffett Field, CA, 94035, USA
[10] SETI Institute, 189 Bernardo Avenue, Suite 200, Mountain View, CA 94043, USA
[11] Department of Astronomy, The University of Texas at Austin, Austin, TX 78712, USA
[12] Department of Earth, Atmospheric, and Planetary Sciences, Massachusetts Institute of Technology, 77 Massachusetts Avenue, Cambridge, MA 02139, USA
[13] Department of Aeronautics and Astronautics, Massachusetts Institute of Technology, 125 Massachusetts Avenue, Cambridge, MA 02139, USA
[14] Department of Astrophysical Sciences, Princeton University, 4 Ivy Lane, Princeton, NJ 08544, USA
[15] Astronomy Department, University of Washington, Seattle, WA 98195, USA
[16] Oukaimeden Observatory, High Energy Physics and Astrophysics Laboratory, Cadi Ayyad University, Marrakech, Morocco
[17] UR Astrobiology, Université de Liège, 19C Allée du 6 Août, B-4000 Liège, Belgium
[18] Caltech/IPAC—NASA Exoplanet Science Institute 1200 E. California Avenue, Pasadena, CA 91125, USA
[19] Observatoire de l'Université de Genève, 51 chemin des Maillettes, 1290 Versoix, Switzerland
[20] STAR Institute, Université de Liège, Allée du 6 Août 17, B-4000 Liège, Belgium
[21] SGT, Inc./NASA AMES Research Center, Mailstop 269-3, Bldg T35C, P.O. Box 1, Moffett Field, CA 94035, USA
[22] Proto-Logic Consulting LLC, Washington, DC 20009, USA
[23] Department of Physics and Astronomy, Vanderbilt University, Nashville, TN 37235, USA
[24] American Association of Variable Star Observers, 49 Bay State Road, Cambridge, MA 02138, USA
[25] Noqsi Aerospace, Ltd., 15 Blanchard Avenue, Billerica, MA 01821, USA
[26] Department of Astronomy and Astrophysics, University of California, Santa Cruz, CA 95064, USA
[27] Nicolaus Copernicus Astronomical Center, Polish Academy of Sciences, ul. Rabiańska 8, 87-100 Toruń, Poland
[28] Department of Physics, Southern Connecticut State University, 501 Crescent Street, New Haven, CT 06515, USA
[29] Deptartment of Physics & Astronomy, Swarthmore College, Swarthmore, PA 19081, USA
[30] Department of Physics and Astronomy, University of Louisville, Louisville, KY 40292, USA
[31] DTU Space, National Space Institute, Technical University of Denmark, Elektrovej 327, DK-2800 Lyngby, Denmark
[32] Brorfelde Observatory, Observator Gyldenkernes Vej 7, DK-4340 Tølløse, Denmark
[33] Department of Physics and Astronomy, University of North Carolina at Chapel Hill, Chapel Hill, NC 27599, USA
[34] School of Physics and Astronomy, Raymond and Beverly Sackler Faculty of Exact Sciences, Tel Aviv University, Tel Aviv 6997801, Israel
[35] Department of Astronomy, The University of Tokyo, 7-3-1 Hongo, Bunkyō, Tokyo 113-8654, Japan
[36] Instituto de Astrofísica de Canarias (IAC), E-38205 La Laguna, Tenerife, Spain
[37] Departamento de Astrofísica, Universidad de La Laguna (ULL), E-38206 La Laguna, Tenerife, Spain
[38] Cavendish Laboratory, University of Cambridge, JJ Thomson Avenue, Cambridge CB3 0H3, UK
[39] JST, PRESTO, 7-3-1 Hongo, Bunkyo-ku, Tokyo 113-0033, Japan
[40] Astrobiology Center, 2-21-1 Osawa, Mitaka, Tokyo 181-8588, Japan
[41] National Astronomical Observatory of Japan, 2-21-1 Osawa, Mitaka, Tokyo 181-8588, Japan
[42] Exoplanets and Stellar Astrophysics Laboratory, Code 667, NASA Goddard Space Flight Center, Greenbelt, MD 20771, USA
[43] Department of Physics, Fisk University, 1000 17th Avenue North, Nashville, TN 37208, USA
[44] Dunlap Institute for Astronomy and Astrophysics, University of Toronto, Toronto, ON M5S 3H4, Canada
Received 2019 January 26; revised 2019 August 15; accepted 2019 August 27; published 2019 October 10

[45] Juan Carlos Torres Fellow.
[46] NASA Sagan Fellow.
[47] Formerly Wyle Labs/NASA Ames Research Center.
[48] Kavli Fellow.
[49] NASA Hubble Fellow.
[50] NSF Graduate Research Fellow.

Abstract

We report the *Transiting Exoplanet Survey Satellite* detection of a multi-planet system orbiting the $V = 10.9$ K0 dwarf TOI-125. We find evidence for up to five planets, with varying confidence. Three transit signals with high signal-to-noise ratio correspond to sub-Neptune-sized planets (2.76, 2.79, and 2.94 $R_{\oplus}$), and we statistically validate the planetary nature of the two inner planets ($P_b = 4.65$ days, $P_c = 9.15$ days). With only two transits observed, we report the outer object ($P_{.03} = 19.98$ days) as a planet candidate with high signal-to-noise ratio. We also detect a candidate transiting super-Earth (1.4 $R_{\oplus}$) with an orbital period of only 12.7 hr and a candidate Neptune-sized planet (4.2 $R_{\oplus}$) with a period of 13.28 days, both at low signal-to-noise ratio. This system is amenable to mass determination via radial velocities and transit-timing variations, and provides an opportunity to study planets of similar size while controlling for age and environment. The ratio of orbital periods between TOI-125 b and c ($P_c/P_b = 1.97$) is slightly lower than an exact 2:1 commensurability and is atypical of multiple planet systems from *Kepler*, which show a preference for period ratios just wide of first-order period ratios. A dynamical analysis refines the allowed parameter space through stability arguments and suggests that despite the nearly commensurate periods, the system is unlikely to be in resonance.

Unified Astronomy Thesaurus concepts: Transit photometry (1709); Mini Neptunes (1063); Super Earths (1655); Exoplanets (498)

Supporting material: animation, data behind figure

1. Introduction

NASA's *Transiting Exoplanet Survey Satellite* (*TESS;* Ricker et al. 2015) is an all-sky survey, the primary objective of which is to discover and characterize transiting planets smaller than Neptune orbiting the nearest and brightest stars in the sky. While the space-based transit survey carried out by *Kepler* (Borucki et al. 2010) led to breakthroughs in our understanding of the occurrence rates of planetary systems (e.g., Fressin et al. 2013) and the various dynamical configurations of multi-planet systems (e.g., Lissauer et al. 2011b; Fabrycky et al. 2014), *TESS* is designed to discover the planetary systems most amenable to detailed characterization through follow-up observations. Typical *TESS* planet hosts will be several magnitudes brighter than those from *Kepler* (Sullivan et al. 2015; Barclay et al. 2018; Huang et al. 2018b), and these statistically rare systems are amenable to the most precise radial-velocity (RV) mass measurements and more efficient atmospheric characterization. This expectaction is borne out by the experience of the *K2* mission (Howell et al. 2014), which surveyed a larger area of sky than *Kepler* and discovered a number of bright planetary systems like those expected from *TESS* (see, e.g., Rodriguez et al. 2018a, and the overview presented therein). *TESS* should also detect objects that are intrinsically rare, such as events occurring on astronomically short timescales, or the unlikely outcomes of dynamical interactions. Further study of these benchmark objects may lead to breakthroughs in our understanding of the fundamental processes that govern the formation and evolution of planetary systems.

Data from just the first *TESS* observing sector (27.4 days, or two spacecraft orbits) have already begun to fulfill this promise. A 2.1$R_{\oplus}$ planet transiting the fifth-magnitude star π Mensae already has a mass measurement (4.8 $M_{\oplus}$) because the star was previously known to host a long-period giant planet and there exist extensive archival RV measurements (Gandolfi et al. 2018; Huang et al. 2018a). The star is one of the very brightest known to host a transiting planet, which will enable further detailed characterization. A second system (LHS 3844; Vanderspek et al. 2019) is an ultra-short period (USP) Earth-sized planet ($R_p = 1.32\,R_{\oplus}$) in an 11 hr orbit around a late-M dwarf 15 pc away. It is one of the nearest planetary systems, and in many respects the USP planet that is most amenable to follow-up studies. The remaining 25 observing sectors in the two-year prime *TESS* mission will survey additional bright stars, some for longer periods of time, and will lead to the discovery of many more benchmark planetary systems.

Among the myriad discoveries from the *Kepler* mission, the detection of systems of multiple transiting planets and the subsequent study of their ensemble properties remain among the most impactful results (e.g., Steffen et al. 2010; Latham et al. 2011; Lissauer et al. 2011a). Multi-planet transiting systems allow investigations of formation and evolution processes through measurements of mutual inclinations, adjacent planet sizes, planet spacings, stellar obliquities, mass measurements via transit-timing variations (TTVs), and more. Given the prevalence of multi-transiting systems, *TESS* will build upon the *Kepler* legacy by discovering the nearest and brightest such systems, as well as the rare examples.

In this paper, we present the discovery and validation of a system of multiple transiting planets orbiting the star TIC 52368076, which has been assigned *TESS* Object of Interest (TOI) number TOI-125. The proposed architecture of the system is illustrated in Figure 1. We identify three candidates with high signal-to-noise ratio (S/N) transits (filled circles), as well as two low-S/N candidates (open circles), one of which is a USP terrestrial candidate.

We describe the analysis of data from *TESS*, ground-based follow-up, and archival imaging in Section 2, fit a global model to all available data in Section 3, present a statistical validation of the planets in Section 4, investigate the dynamics in Section 5, and discuss the properties of the system and prospects for future characterization in Section 6.

2. Data and Analysis

2.1. TESS *Photometry*

TIC 52368076 was observed by *TESS* in the first two sectors of the prime mission (2018 July 25 through 2018 September 21) on CCD 1 of Camera 3 in Sector 1 and CCD 2 of Camera 3 in Sector 2. The CCDs obtain images at a two-second cadence, which are summed on board the spacecraft to produce images with the appropriate effective exposure time. All stars within the *TESS* field of view are observed with an effective exposure time of 30 minutes, but a subset of stars (including TIC 52368076)

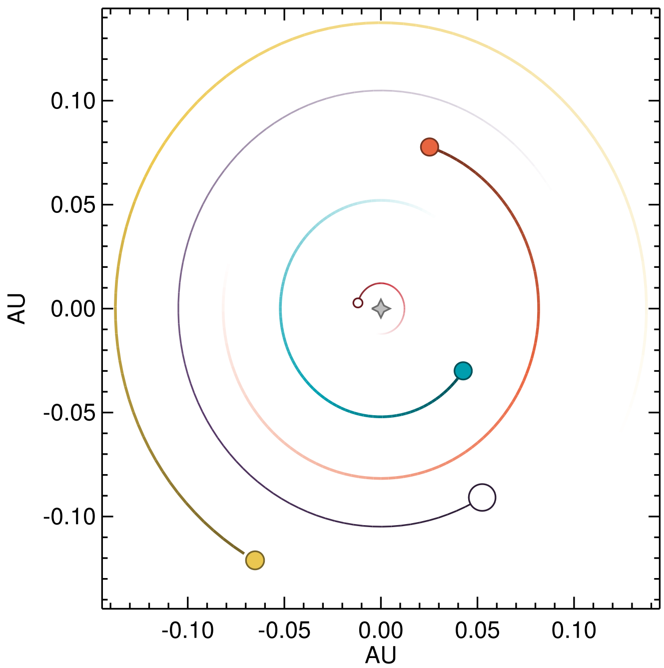

Figure 1. A top-down view of the TOI-125 planetary system. The planet sizes are drawn to scale relative to each other. The low-S/N candidates (TOI-125.04 and .05) are shown as open circles, while the high-S/N candidate and validated planets are filled circles. We note that the derived size of .05 is very uncertain because its transit is grazing ($R_{.05} = 8.8^{+4.7}_{-4.4}$; $b = 1.056^{+0.055}_{-0.057}$). Moreover, planets like TOI-125.05 are a priori likely to be small; if real, its true size is probably smaller than this formal estimate. An animated version of this figure is available, showing the orbital motion of the system throughout *TESS* Sectors 1 and 2.

(An animation of this figure is available.)

were preselected, primarily on the basis of planet detectability (Stassun et al. 2018), for data to also be returned to Earth at a two-minute cadence.

The two-minute data were reduced with the Science Processing Operations Center (SPOC) pipeline (Jenkins et al. 2015, 2016), adapted from the pipeline for the *Kepler* mission at the NASA Ames Research Center (Jenkins et al. 2010). Two transit signals were strongly detected with periods of 4.65 and 9.15 days and an S/N of 20.1 and 16.4, respectively. These candidates were assigned identifiers TOI-125.01 and TOI-125.02 by the *TESS* team. An additional signal, TOI-125.03, was detected with only two transit-like events at a period of 19.98 days and an S/N of 9.8. (Unfortunately, TOI-125 will not be observed again during the two-year prime mission.) In the analyses that follow, we use the pre-search data conditioning (PDC) light curve from SPOC (see Stumpe et al. 2012). Figure 2 shows the PDC light curve after flattening (we note that the raw PDC light curve looks nearly identical, as the star is photometrically very quiet). Interruptions in data acquisition occur at the perigee of each *TESS* orbit (once every 13.7 days) and last approximately 1 day, during which time the spacecraft reorients to downlink data. The second orbit of Sector 1 included a two-day period during which the data were of lower quality due to a one-time occurrence of abnormally unstable spacecraft pointing. The worst of these data were flagged by SPOC and removed, which can be seen as an underdensity of points in Figure 2 just before BTJD 1350. Fortuitously, none of the transits of these three candidates occurred at this time. During Sectors 1 and 2, the spacecraft thrusters were fired periodically (approximately every 2.5 days) to reduce the speed of the reaction wheels, allowing them to operate at frequencies that introduced less pointing jitter. In intervals of 10–15 minutes around these "momentum dumps," we removed data from our analysis.

2.2. Additional Planet Candidates

Following the convention from *Kepler*, we adopt a formal significance threshold of 7.1σ, and the three candidate planets described above are the only formally significant periodic signals in the data. However, we do detect lower S/N transit-like signals at two other periods. The first, TOI-125.04, has a period of 0.52854 days and a depth of 180 ppm (5.2σ), which corresponds to a planet radius of $1.36\,R_\oplus$ (see Figure 3). The second, TOI-125.05, was detected at a period of 13.2780days and a depth of 675 ppm (5.1σ). If this were a central transit, it would correspond to a planet radius of $\sim 2.2\,R_\oplus$, but it is best modeled as a grazing transit (see Figure 4), so when unconstrained by other data, even giant planets are allowed. However, our CORALIE spectroscopy (Section 2.6) rules out the most massive companions, and we ultimately derive a radius of $\sim 4.2\,R_\oplus$, still with large error bars. Given the low S/N of these candidates and the non-Gaussian noise of the first *TESS* sectors (e.g., the systematics related to spacecraft pointing discussed in Section 2.1), we do not consider the signals strong enough to be validated as planets, particularly TOI-125.05, which only shows four transits of varying quality. Nevertheless, the presence of three other strong planet candidates makes these signals more intriguing, and we note them here so that they can be taken into account during follow-up observations and subsequent analysis of the first three candidates.

2.3. Ground-based Photometry

Given the 21″ *TESS* pixels and a point spread function (PSF) that is a few pixels wide, the light from an individual star on the detector can extend well beyond 1′. In order to capture most of the light from the target star, the *TESS* photometric apertures must also be large. Therefore, even apparently isolated stars may be contaminated by relatively distant neighbors, with the exact contamination fraction depending upon the aperture choice and the magnitudes of the stars (see, e.g., the size of the PSF in the *TESS* image of TOI-125 shown in Figure 5). If a neighboring star is an eclipsing binary (EB), deep eclipses can be diluted to resemble shallow planetary transits. While previous experience with *Kepler* candidate multi-planet systems shows the vast majority to be real planets (e.g., Lissauer et al. 2012), the larger *TESS* pixels and aperture create more opportunity for unassociated EBs to contaminate real planetary systems (producing candidate multi-planet systems containing both real planets and false positives). Centroid analysis of the *TESS* difference images (comparing the in-transit to out-of-transit flux) is often effective at identifying nearby EBs, but transit signals with a small number of events or contaminants within about a pixel might not be robustly detected. We therefore observed TOI-125 with ground-based facilities at predicted times of transit to search for deep eclipses in nearby stars. We enumerate these observations in Table 1. In order to produce the 1 mmag events of TOI-125 b, c, or .03 with even a 50% eclipse, a nearby star must be no more than 6.9 magnitudes fainter (and fully blended in the *TESS* aperture). Of the *Gaia* DR2 sources, only one nearby star is bright enough, but at a distance of 75″ (to the SSW), it is not fully blended within the *TESS* aperture (see Figure 5). Nonetheless, we search this and other nearby stars for evidence

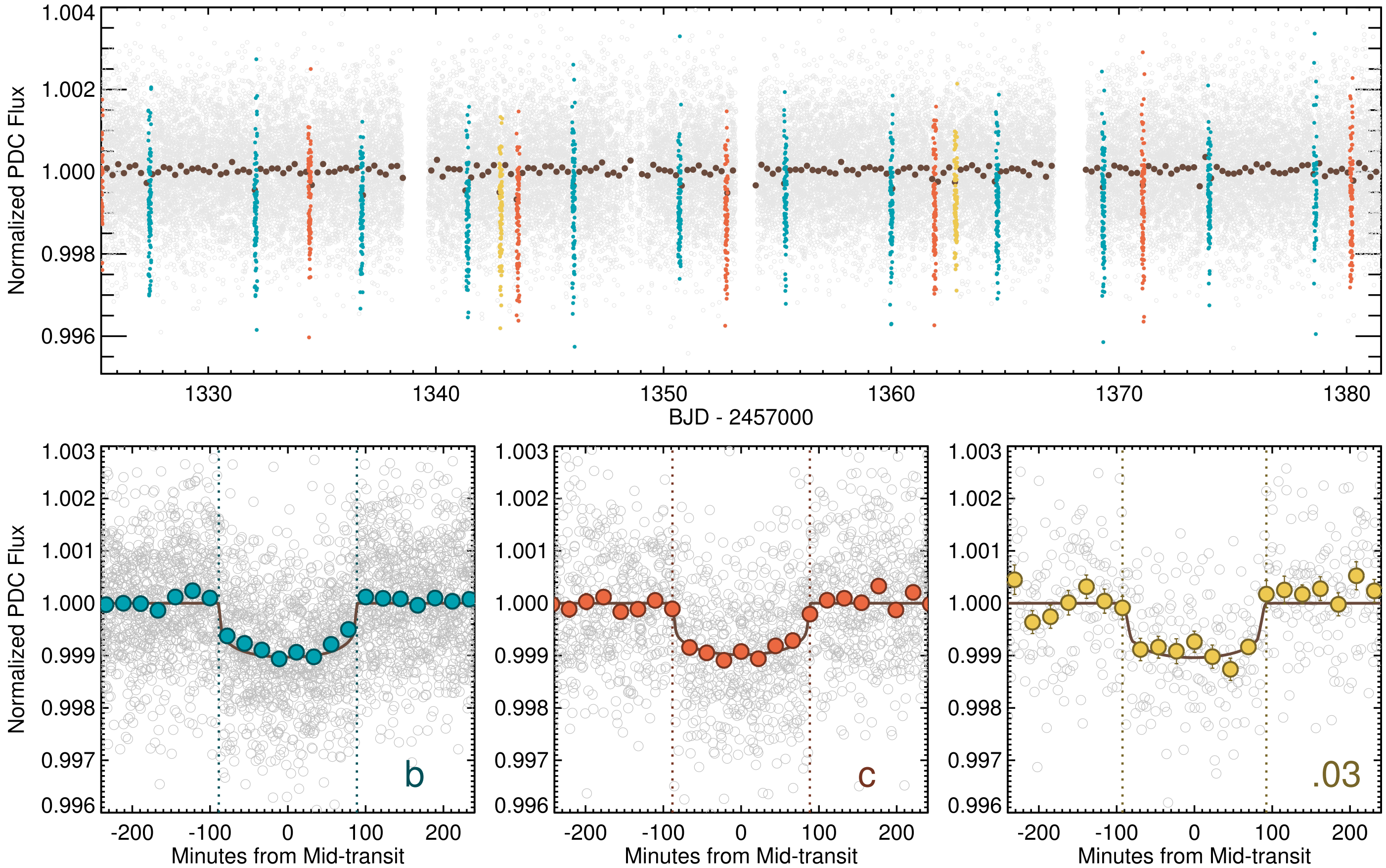

Figure 2. (Top) The full *TESS* light curve of TOI-125 from Sectors 1 and 2. The light curve has been flattened using the technique from Vanderburg et al. (2016). We show the individual two-minute cadence measurements (open gray circles) and the same data in six-hour bins (brown circles). In-transit cadences corresponding to the inner, middle, and outer planets are plotted with blue, orange, and yellow circles, respectively. (Bottom) The phase-folded transits of each planet, with individual observations (open gray circles) and binned data (filled colored circles, chosen to have eight bins per transit duration). The best-fit EXOFASTv2 models are plotted in brown. Vertical dotted lines indicate the full transit durations.

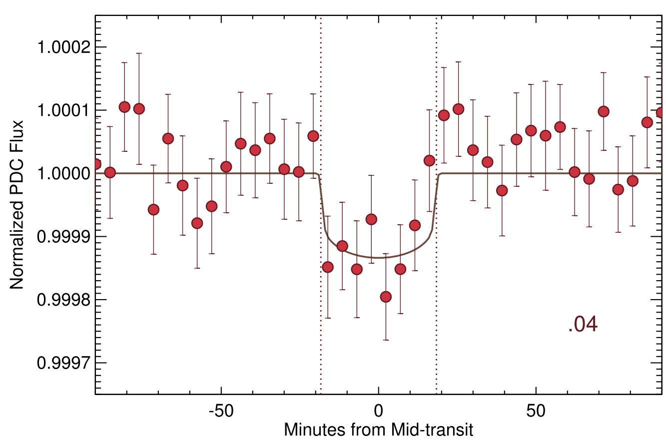

Figure 3. The phase-folded transit of the candidate USP super-Earth, TOI-125.04. We plot the binned photometry (filled red circles), as the individual two-minute data extend far beyond the *y*-axis range. The best-fit EXOFASTv2 model is plotted in brown. Vertical dotted lines indicate the full transit duration.

of deep eclipses, and we find no indication of contamination from nearby EBs in our timeseries observations.

2.4. Archival Imaging

Ground-based photometric follow-up can rule out the presence of EBs at modest separations, but a physically unassociated background star within a few arcseconds of the location of TOI-125 could plausibly produce a transit-like signal that would not be resolved as a separate source in the few-arcsecond PSFs of follow-up images. To address this possibility, we examine archival images, in which the proper motion of TOI-125 has carried it away from its current location. Figure 5 shows the *TESS* image from Sector 1 along with images from the ESO/SERC Southern Sky Atlas (SERC-J; taken in 1975) and the Anglo-Australian Observatory Second Epoch Survey (AAO-SES; 1993). The most constraining of these is the SERC-J image, enlarged in the left panel. The proper motion of $\mu_\alpha = -120$ mas yr^{-1} and $\mu_\delta = -123$ mas yr^{-1} leads to motion of $1\farcs7$ per decade; in the 43 yr since the SERC-J image was obtained, TOI-125 has moved $7\farcs4$. A background source at the current location of TOI-125 should be seen as elongation of the PSF or a nearly resolved source. There is no indication of such features in either the blue-sensitive SERC-J or the red-sensitive AAO-SES images, so we conclude that there is no background source coincident with the present-day location of TOI-125.

2.5. High Angular Resolution Imaging

Ground-based photometry rules out EBs at modest separations and archival imaging rules out background sources, but there may still be a bound stellar companion at small angular separation. An unresolved companion may itself be an EB responsible for one of the transit-like signals, but even if it is

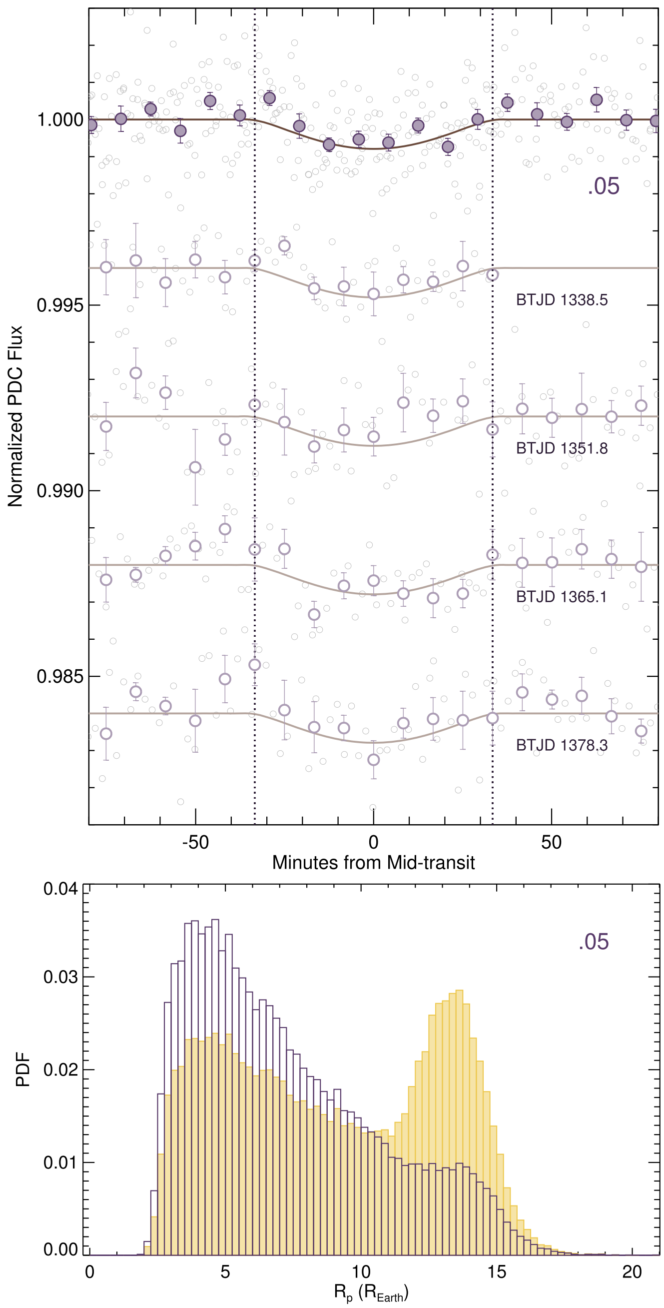

Figure 4. Top: the phase-folded and individual transits of the low-S/N candidate TOI-125.05. Bottom: the EXOFASTv2 marginalized posterior distribution for $R_{.05}$ (filled yellow bars), and the revised distribution when constrained by the CORALIE RVs and a mass–radius relationship (open purple bars).

Table 1
Ground-based Photometry of TOI-125

Planet	Facility	Filter	Type[a]	T_c BJD$_{TDB}$[b]
b	TRAPPIST-S 0.6 m[c]	z′	F	1378.6245
b	LCO-SS 0.4 m	i′	I	1383.2783
b	SLR2 0.5 m	V	E	1383.2783
b	SLR2 0.5 m	V	I	1392.5860
b	LCO-SAAO 1.0 m	z_s	I	1392.5860
b	LCO-SAAO 1.0 m	i′	I	1406.5475
c	MKO CDK700 0.7 m	r′	I	1371.0589
c	LCO-SAAO 1.0 m	z_s	F	1389.3608
c	IRSF 1.4 m	J, H, K_s	F	1398.5117
c	SSO/Europa 1.0 m[c]	z′	F	1407.6626
.03	LCO-CTIO 1.0 m	i′	I	1442.7549

Notes. Each ground-based follow-up light curve is listed here, along with the predicted time of transit. Because the transits are so shallow (<1 part per thousand for all three candidates), the ground-based data do not confidently detect the transits, and we do not include them in the global fit (Section 3). No nearby EBs were detected.
[a] F: full transit (covering ingress and egress); I: ingress only; E: egress only.
[b] Times of conjunction are given in the standard *TESS*-reported format, which is BJD$_{TDB}$ − 2,457,000.
[c] TRAPPIST (Jehin et al. 2011); SPECULOOS (Delrez et al. 2018).

not, the dilution must be taken into account in the light-curve fit in order to derive accurate radii (e.g., Buchhave et al. 2011), and the presence (or absence) of a binary companion can help us understand the formation of compact planetary systems (e.g., Kraus et al. 2016). Fortunately, bound companions to *TESS* planet hosts will be more easily revealed by high-resolution imaging than the typical *Kepler* system because they are, on average, more nearby (e.g., Ciardi et al. 2015; Matson et al. 2019).

We searched for close companions to TOI-125 in *I* band using the HRCam speckle imager on the 4.1 m Southern Astrophysical Research (SOAR) telescope (Tokovinin 2018; Ziegler et al. 2018b) on 2018 September 25 UT, in narrow-band $Br\gamma$ using the NaCo adaptive optics imager (Lenzen et al. 1998; Rousset et al. 1998) on the 8 m UT1 of the VLT on 2018 October 23, and simultaneously in *R* and *I* band using the DSSI speckle imager (Horch et al. 2009, 2012) on the 8 m Gemini South Telescope on 2018 October 31 UT. We detected no companions in any of these images down to contrast ratios of more than 5 magnitudes outside of 0.″2 of TOI-125. Outside of 1.″5, *Gaia* DR2 can exclude the presence of stellar sources bright enough to cause the ∼1 mmag transit signals when blended with TOI-125 (Ziegler et al. 2018a). The 5σ contrast curves are shown in Figure 6.

2.6. Reconnaissance Spectroscopy

We obtained three spectra with the CORALIE spectrograph (Queloz et al. 2000; Pepe et al. 2018) on the Swiss Euler 1.2 m telescope of the ESO-La Silla Observatory (Chile) between UT 2018 September 07 and 2018 October 02. We used simultaneous Fabry-Pérot calibration for intrinsic drift measurement. The S/N per pixel of the individual spectra was ∼20. Data were reduced using an adapted version of the HARPS pipeline: the average stellar line profiles, or cross-correlation functions (CCFs), were computed by cross-correlating the CORALIE spectra with a weighted binary G2 mask from which various tellurics and interstellar medium (ISM) lines were removed (Pepe et al. 2002). We see no evidence for multiple peaks in the CCF, suggesting that TOI-125 does not have a bright unresolved stellar companion. The RVs, reported in Table 2, show no significant velocity variation, and we use this to refine the allowed sizes for candidate TOI-125.05 (see Section 2.2 and Figure 4). We derive spectroscopic parameters using SpecMatch (Petigura et al. 2015; Yee et al. 2017), and find $T_{\rm eff} = 5187 \pm 110$ K, $\log g = 4.52 \pm 0.12$, $[{\rm Fe/H}] = 0.06 \pm 0.09$, and $v \sin i_\star < 2\ {\rm km\ s^{-1}}$. We use these values as starting guesses for our global model, and apply the derived [Fe/H] as a prior (see Section 3).

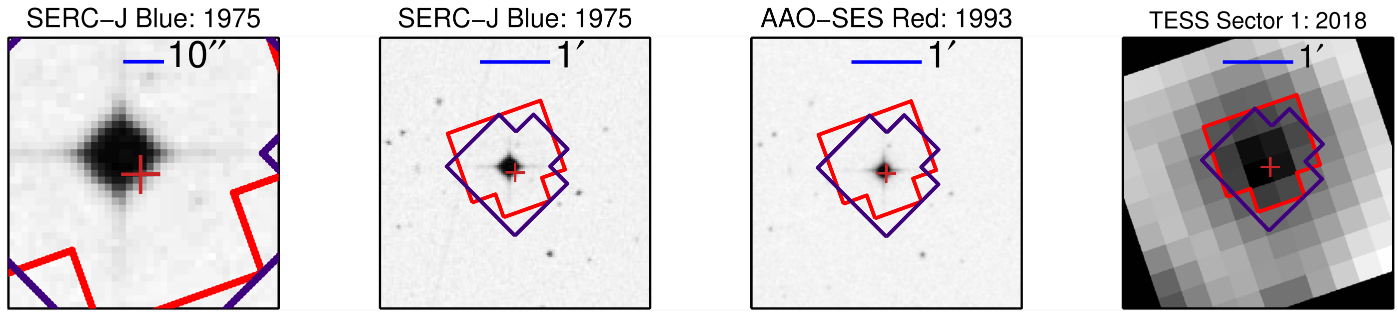

Figure 5. Archival images of TOI-125 (left three panels) and the *TESS* image from Sector 1 (right). Photometric apertures used in Sectors 1 (red outline) and 2 (blue outline) are also shown. The proper motion of the star has led to motion of ∼7.″4 in 43 yr. Its current location (red cross) is marked in all images, and we detect no background sources at this location in previous epochs.

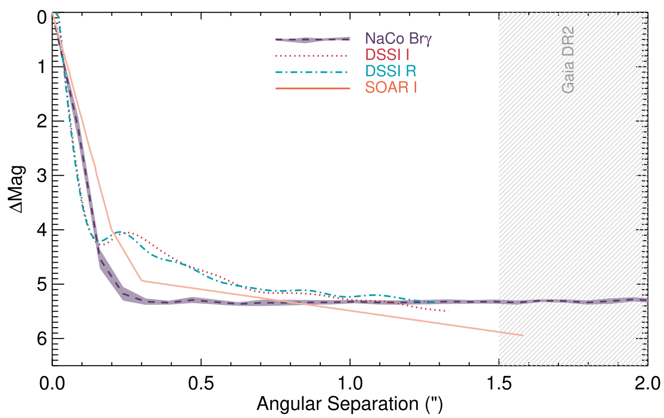

Figure 6. We show the 5σ contrast curves for the high-resolution imaging observations of TOI-125: SOAR HRCam speckle imaging in *I* band (solid orange line); Gemini DSSI speckle imaging in *R* band (blue dot–dashed line) and *I* band (red dotted line); and Very Large Telescope (VLT) NaCo AO imaging in *Brγ* (purple dashed line, with azimuthal scatter shown as a light purple shaded region). We exclude companions fainter by up to about 5 magnitudes in all bands outside a few tenths of an arcsecond. *Gaia* DR2 excludes the presence of wider companions bright enough to produce the ∼1 mmag signals of the high-S/N candidates.

Table 2
CORALIE Radial Velocities of TOI-125

BJD_{TDB}	RV (km s^{-1})	σ_{RV} (km s^{-1})	BIS (km s^{-1})	σ_{BIS} (km s^{-1})
2458368.687418	11.071	0.011	−0.082	0.011
2458379.908910	11.047	0.018	−0.077	0.018
2458393.713423	11.064	0.013	−0.073	0.013

Note. Radial velocities and bisector span measurements from CORALIE observations (Section 2.6). We detect no variation in either quantity, consistent with expectations for a quiet star orbited by small planets.

3. EXOFASTv2 Global Fit

To gain a full understanding of the system parameters, we globally fit the available photometric and spectroscopic data using the publicly available exoplanet modeling suite, EXOFASTv2 (Eastman et al. 2013; Eastman 2017). Specifically, we fit the *TESS* light curves from observing Sectors 1 and 2 for planets b, c, and candidates .03, .04, and .05 (see Figures 2–4), while constraining the host star parameters using the spectral energy distribution (SED) and the MESA Isochrones and Stellar Tracks (MIST) stellar isochrones (Paxton et al. 2011, 2013, 2015; Choi et al. 2016; Dotter 2016). The broadband photometry is given in Table 3 and shown along with the final model in Figure 7. We enforce Gaussian priors $T_{\rm eff} = 5187 \pm 110$ K and $[Fe/H] = 0.06 \pm 0.09$ dex

Table 3
Literature Properties for TOI-125

Parameter	Description	Value	Source
Other Identifiers	TIC 52368076		
	TYC 88956-00192-1		
	2MASS J01342273-6640328		
	Gaia DR2 4698692744355471616		
α_{J2000}	R.A.	01:34:22.735	1
δ_{J2000}	decl.	−66:40:32.95	1
T	*TESS T* mag	10.138 ± 0.017	6
B_T	Tycho B_T mag	11.882 ± 0.077	2
V_T	Tycho V_T mag	11.102 ± 0.065	2
B[a]	APASS Johnson *B* mag	11.701 ± 0.025	3
V	APASS Johnson *V* mag	10.892 ± 0.016	3
G	*Gaia G* mag	10.7180 ± 0.0004	1
g'	APASS Sloan g' mag	11.268 ± 0.019	3
r'	APASS Sloan r' mag	10.458 ± 0.041	3
i'	APASS Sloan i' mag	10.662 ± 0.017	3
J	2MASS *J* mag	9.466 ± 0.02	4
H	2MASS *H* mag	9.112 ± 0.03	4
K_S	2MASS K_S mag	8.995 ± 0.02	4
WISE1	*WISE1* mag	8.945 ± 0.03	5
WISE2	*WISE2* mag	9.006 ± 0.03	5
WISE3	*WISE3* mag	8.944 ± 0.03	5
WISE4	*WISE4* mag	8.613 ± 0.262	5
μ_α	PM in R.A. (mas yr^{-1})	−119.800 ± 0.066	1
μ_δ	PM in decl. (mas yr^{-1})	−122.953 ± 0.080	1
π	Parallax (mas)	8.976 ± 0.036	1
RV	Systemic RV (km s^{-1})	11.062 ± 0.012	7

Note.
[a] The uncertainties of the photometry have a systematic error floor applied. However, the global fit requires a significant scaling of the uncertainties quoted here to be consistent with our model, suggesting they are still significantly underestimated for one or more of the broadband magnitudes.

References. (1) *Gaia* Collaboration et al. (2018); (2) Høg et al. (2000); (3) Henden et al. (2016); (4) Cutri et al. (2003); (5) Cutri et al. (2014); (6) Stassun et al. (2018); (7) this work.

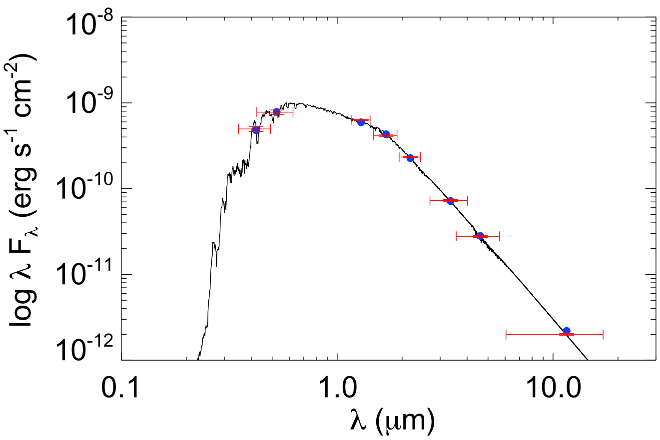

Figure 7. The SED fit from EXOFASTv2 for TOI-125. The red points are the observed values at the corresponding passbands and the blue points are the predicted integrated fluxes. The horizontal red error bars represent the width of the bandpasses and the vertical errors represent the 1σ uncertainties. The final model fit is shown as a solid black line.

Table 4
TOI-125 Stellar Parameters: Median Values and 68% CI

Parameter	Units	Values
Stellar Parameters:		
M_*	Mass ($M_\odot$)	$0.871^{+0.046}_{-0.040}$
R_*	Radius ($R_\odot$)	$0.852^{+0.017}_{-0.016}$
L_*	Luminosity ($L_\odot$)	$0.509^{+0.024}_{-0.025}$
ρ_*	Density (cgs)	1.99 ± 0.15
$\log g$	Surface gravity (cgs)	4.518 ± 0.027
$T_{\rm eff}$	Effective temperature (K)	5282^{+67}_{-75}
[Fe/H]	Metallicity (dex)	$0.069^{+0.083}_{-0.081}$
Age	Age (Gyr)	$6.6^{+4.6}_{-4.2}$
EEP	Equal evolutionary point	348^{+28}_{-27}
A_V	*V*-band extinction (mag)	$0.024^{+0.019}_{-0.017}$
$\sigma_{\rm SED}$	SED photometry error scaling	$2.45^{+1.1}_{-0.62}$
π	Parallax (mas)	$8.975^{+0.099}_{-0.100}$
d	Distance (pc)	$111.4^{+1.3}_{-1.2}$

from the analysis of the CORALIE spectra. We also place a conservative Gaussian prior on the parallax from *Gaia* DR2 of 8.976 ± 0.1 mas because all possible uncertainties should total to less than 0.1 mas (*Gaia* Collaboration et al. 2016, 2018). Last, we enforce an upper limit on the extinction of $A_V = 0.0521$ from the Schlegel Galactic dust reddening and extinction maps (Schlegel et al. 1998). All other parameters were allowed to vary without prior constraints. We allowed an error-scaling term for the SED photometry (reported in Table 4) and a variance term for each sector of the *TESS* photometry (Table 5). Limb-darkening parameters are interpolated using the current $\log g$, $T_{\rm eff}$, and [Fe/H] at each step and the limb-darkening tables of Claret (2017). We adopt the strict convergence criteria recommended by Ford (2006) in order to ensure that the global minimum has been identified and covariances are well characterized: the Gelman–Rubin statistic for all parameters must be lower than 1.01, and the number of independent draws (chain length divided by correlation length) must exceed 1000. We ran a fit that allowed TTVs but found no significant TTVs and no changes to the derived parameters, and therefore adopted the solution that assumes periodic ephemerides for simplicity. We also ran fits including only the two, three, or four strongest signals, and we found stellar and planetary results fully consistent with the five-planet solution. Because inclusion of the two more marginal candidates does not affect our conclusions about TOI-125 b, c, and .03, we present the five-planet fit here. The final system parameters determined by the EXOFASTv2 fit, including predicted masses using the relations of Chen & Kipping (2017), are shown in Tables 4 and 5. We again refer to the top view of the system architecture in Figure 1.

4. Statistical Validation with VESPA

We used the `vespa` package (Morton 2015) to assess the statistical likelihood that the transits of TOI-125 b and c are caused by planets rather than false positives. `vespa` simulates stellar and planetary systems to generate transits (and eclipses) to compare against the observed data of TOI-125. Rejecting systems that are inconsistent with the observations, `vespa` then calculates the false-positive probability (FPP) for each candidate. The FPP depends on the transit shape, the position of the star on the sky (to assess the likelihood of background blends), the stellar parameters (which hold information not only on transit and eclipse shapes, but also on the likelihood of stellar companions), the extent to which nearby EBs can be excluded by high-resolution imaging, and the presence or absence of features in the light curve that might indicate the presence of a binary (such as depth differences in alternating transits or the presence of a secondary eclipse). We therefore provide to `vespa` the sky coordinates, stellar parameters, literature photometry, high-resolution imaging contrast curves, and the flattened *TESS* light curve. Our RVs rule out an EB (as opposed to a blended background or hierarchical EB).

After running `vespa`, we adjusted the FPP by excluding the scenario in which a direct EB companion to TOI-125 causes one of the transit signals. The resulting FPPs are 6×10^{-5} and 9×10^{-5} for TOI-125.01 and .02, respectively. Note that we did not remove the contribution from background EBs even though our inspection of the archival imaging suggests that there are no background stars at the current location of TOI-125; the FPPs would be even lower with this adjustment. We therefore conclude that these are statistically validated planets, and now refer to them as TOI-125 b and c. We do not attempt to validate TOI-125.04 and .05 because `vespa` does not assess the likelihood that a signal is an instrumental false alarm, and we cannot fully exclude this possibility given the low S/N of these events. Similarly, we do not attempt to validate TOI-125.03 despite its high S/N because we observed only two transits. There is a chance that these could be explained by single transits of two planets, or a single transit plus an instrumental effect.

5. Dynamics

This section considers dynamical aspects of the TOI-125 system, considering the three planets with the highest S/N detections. We first note that TOI-125 b has nonzero eccentricity, but a relatively short timescale for the damping of its eccentricity. As a result, the system is dynamically interesting, suggesting some type of planet–planet interactions. These types of interactions could lead to TTVs (Section 5.1), although they are not observed in the present data set. We also need to consider

Table 5
TOI-125 Planetary and Transit Parameters: Median Values and 68% Confidence Interval

Parameter	Description (Units)	Values				
		Low S/N	Validated	Validated	Marginal	High S/N
		.04	b	c	.05[a]	.03
P	Period (days)	$0.528474^{+0.000040}_{-0.000030}$	$4.65382^{+0.00032}_{-0.00031}$	$9.15067^{+0.00062}_{-0.00069}$	$13.2781^{+0.0020}_{-0.0019}$	$19.9807^{+0.0045}_{-0.0049}$
R_P	Radius ($R_\oplus$)	$1.36^{+0.14}_{-0.16}$	$2.755^{+0.091}_{-0.079}$	2.79 ± 0.10	$8.8^{+4.7}_{-4.4}$	2.94 ± 0.16
T_C	Time of conjunction (BJD_{TDB})	2458350.8394 ± 0.0011	$2458355.35520^{+0.00093}_{-0.00087}$	$2458352.7582^{+0.0014}_{-0.0013}$	$2458365.0560^{+0.0019}_{-0.0020}$	$2458342.8514^{+0.0034}_{-0.0033}$
a	Semimajor axis (au)	$0.01222^{+0.00021}_{-0.00019}$	$0.05210^{+0.00090}_{-0.00082}$	$0.0818^{+0.0014}_{-0.0013}$	$0.1048^{+0.0018}_{-0.0016}$	$0.1376^{+0.0024}_{-0.0022}$
i	Inclination (degrees)	$72.80^{+0.72}_{-0.70}$	$88.99^{+0.70}_{-0.81}$	$88.52^{+0.32}_{-0.19}$	$87.70^{+0.15}_{-0.14}$	$88.753^{+0.080}_{-0.081}$
e	Eccentricity	⋯	$0.183^{+0.14}_{-0.098}$	$0.065^{+0.067}_{-0.046}$	$0.037^{+0.046}_{-0.027}$	$0.075^{+0.056}_{-0.051}$
ω_*	Argument of periastron (degrees)	⋯	-91^{+57}_{-56}	90^{+97}_{-98}	50 ± 120	90^{+100}_{-110}
$e\cos\omega_*$		⋯	-0.00 ± 0.17	$-0.000^{+0.055}_{-0.054}$	$0.000^{+0.036}_{-0.034}$	0.000 ± 0.063
$e\sin\omega_*$		⋯	$-0.114^{+0.057}_{-0.098}$	$0.014^{+0.075}_{-0.042}$	$0.001^{+0.037}_{-0.031}$	$0.011^{+0.072}_{-0.053}$
$\langle F \rangle$	Incident flux (10^9 erg $s^{-1}cm^{-2}$)	4.63 ± 0.25	$0.243^{+0.017}_{-0.019}$	$0.1026^{+0.0056}_{-0.0055}$	$0.0627^{+0.0034}_{-0.0033}$	$0.0362^{+0.0020}_{-0.0019}$
T_{eq}	Equilibrium temperature (K)	2126^{+28}_{-29}	1029 ± 14	821 ± 11	$725.8^{+9.5}_{-9.8}$	$633.5^{+8.3}_{-8.5}$
R_P/R_*	Radius of planet in stellar radii	$0.0146^{+0.0014}_{-0.0016}$	$0.02962^{+0.00077}_{-0.00063}$	$0.02998^{+0.00087}_{-0.00086}$	$0.095^{+0.051}_{-0.047}$	$0.0317^{+0.0015}_{-0.0016}$
a/R_*	Semimajor axis in stellar radii	3.085 ± 0.077	13.15 ± 0.33	20.65 ± 0.52	26.47 ± 0.66	34.75 ± 0.87
d/R_*	Separation at mid-transit	3.085 ± 0.077	$14.29^{+1.3}_{-0.97}$	$20.2^{+1.1}_{-1.5}$	$26.4^{+1.1}_{-1.2}$	$34.1^{+2.2}_{-2.5}$
Depth	Flux decrement at mid-transit	$0.000214^{+0.000043}_{-0.000045}$	$0.000877^{+0.000046}_{-0.000037}$	$0.000899^{+0.000053}_{-0.000051}$	0.00123 ± 0.00019	$0.001004^{+0.00010}_{-0.000096}$
τ	Ingress/egress transit duration (days)	$0.00206^{+0.00049}_{-0.00039}$	$0.00376^{+0.00095}_{-0.00024}$	$0.00488^{+0.00070}_{-0.00078}$	$0.0232^{+0.0018}_{-0.0015}$	$0.0086^{+0.0016}_{-0.0014}$
T_{14}	Total transit duration (days)	$0.0255^{+0.0022}_{-0.0027}$	$0.1233^{+0.0025}_{-0.0026}$	$0.1227^{+0.0025}_{-0.0028}$	$0.0464^{+0.0037}_{-0.0030}$	$0.1284^{+0.0055}_{-0.0057}$
T_{FWHM}	FWHM transit duration (days)	$0.0235^{+0.0025}_{-0.0031}$	$0.1192^{+0.0023}_{-0.0024}$	$0.1179^{+0.0026}_{-0.0030}$	$0.0232^{+0.0019}_{-0.0015}$	$0.1198^{+0.0060}_{-0.0063}$
b	Transit impact parameter	$0.912^{+0.023}_{-0.022}$	$0.25^{+0.24}_{-0.17}$	$0.524^{+0.078}_{-0.14}$	$1.056^{+0.055}_{-0.057}$	$0.745^{+0.047}_{-0.060}$
M_P	Predicted mass ($M_\oplus$)	$2.65^{+0.94}_{-0.56}$	$8.5^{+2.8}_{-1.8}$	$8.6^{+2.8}_{-1.9}$	61^{+200}_{-42}	$9.5^{+3.2}_{-2.1}$
K	Predicted RV semi-amplitude (m s^{-1})	$2.19^{+0.78}_{-0.47}$	$3.65^{+1.2}_{-0.80}$	$2.88^{+0.95}_{-0.64}$	18^{+59}_{-13}	$2.45^{+0.84}_{-0.56}$
$\log K$	Log of RV semi-amplitude	$0.34^{+0.13}_{-0.10}$	$0.56^{+0.12}_{-0.11}$	$0.46^{+0.12}_{-0.11}$	$1.26^{+0.63}_{-0.52}$	$0.39^{+0.13}_{-0.11}$
ρ_P	Predicted density (cgs)	$5.9^{+2.0}_{-1.3}$	$2.21^{+0.72}_{-0.47}$	$2.17^{+0.70}_{-0.47}$	$0.69^{+0.92}_{-0.36}$	$2.04^{+0.68}_{-0.44}$
$\log g_P$	Predicted surface gravity	$3.147^{+0.12}_{-0.092}$	$3.04^{+0.12}_{-0.10}$	$3.03^{+0.12}_{-0.10}$	$2.94^{+0.26}_{-0.15}$	$3.03^{+0.12}_{-0.10}$
M_P/M_*	Predicted mass ratio	$0.0000091^{+0.0000033}_{-0.0000020}$	$0.0000291^{+0.0000098}_{-0.0000064}$	$0.0000295^{+0.0000098}_{-0.0000066}$	$0.00021^{+0.00069}_{-0.00015}$	$0.0000325^{+0.000011}_{-0.0000075}$
Wavelength Parameters:		*TESS*				
u_1	linear limb-darkening coeff	0.391 ± 0.037				
u_2	quadratic limb-darkening coeff	0.231 ± 0.036				
Transit Parameters:		*TESS* Sector 1	*TESS* Sector 2			
σ^2	Added variance	$4.0^{+1.8}_{-1.7} \times 10^{-8}$	$1.1 \pm 1.7 \times 10^{-8}$			
F_0	Baseline flux	1.000033 ± 0.000013	1.000074 ± 0.000012			

Notes. We reiterate that TOI-125 b, c, and .03 are high-S/N events; the USP TOI-125.04 is intriguing even though it does not meet our formal significance threshold; and we consider TOI-125.05 a marginal planet candidate but present it for completeness.

[a] The values reported for TOI-125.05 are those from EXOFASTv2 without any RV constraint. We note that when we exclude the solutions that are inconsistent with the CORALIE RVs, the most probable size is $R_P \sim 4.2\ R_\oplus$ (see Figure 4). Moreover, planets like TOI-125.05 are a priori likely to be small; if real, its true size is probably even smaller.

possible instability of the system (Section 5.2), which places additional constraints on the allowed current values of the orbital eccentricities. Finally, we consider the question of mean motion resonances (MMRs), and find that the system is highly unlikely to currently be in a true resonant configuration (Section 5.3).

5.1. Transit-timing Variations

The proximity of TOI-125 b and c to a 2:1 MMR means that their mutual gravitational perturbations add in a nearly coherent manner that can lead to significant and potentially measurable TTVs (e.g., Agol et al. 2005; Holman & Murray 2005). An attempt to model the planets' timing variations in the first two sectors of *TESS* did not yield significant dynamical constraints, as the uncertainty on the transit times from *TESS* is larger than the expected TTVs. Here we briefly consider the prospects for extracting dynamical information by combining the first two sectors of *TESS* observations with future follow-up observations.

To assess the possibility for extracting dynamical information from TOI-125 b and c TTVs, we need to know how the expected TTV signal amplitude compares to the precision of any future transit-time measurements. We employ the analytic TTV model detailed in Hadden et al. (2019) in order to predict the planets' TTV signals and the accompanying dynamical constraints derived from them. Figure 8 shows the TTV signals predicted for b and c, assuming no free eccentricity for either planet[51] and fiducial masses of $3 \times 10^{-5}\,M_*$ for both planets. The resulting TTVs are approximately sinusoidal with amplitudes of $\sim$3 minutes. The planets' TTV signals will, to excellent approximation, simply scale linearly with the planet masses. To estimate the timing precision that might be achieved using *Spitzer*, we scale the S/N from existing transit observations and employ the analytic formulae of Carter et al. (2008) and Price & Rogers (2014), which lead to a per-transit uncertainty of 1 minute. The bottom panel of Figure 8 shows the estimated precision with which the mass of planet c could be measured using the TTV of planet b by obtaining a series of follow-up observations centered on the peaks of the approximately sinusoidal TTV and assuming that transit mid-times are measured with 1σ uncertainties of 1 minute. Precisions approaching $\sim 1 M_\oplus$ are achievable with a series of transit observations consisting of $\sim$3–5 transit-timing measurements made at two or three successive peaks of the TTV signal. However, we note that these mass measurement precisions are based on a TTV model that assumes zero free eccentricity for TOI-125 b and c; relaxing this assumption would significantly increase the mass uncertainty due to the mass-eccentricity degeneracy inherent to TTVs of planets near MMRs (e.g., Lithwick et al. 2012). On the other hand, the combination of TTVs and RVs would provide the strongest possible mass and eccentricity constraints, and in Section 6.1 we argue that the planets should be amenable to RV follow-up.

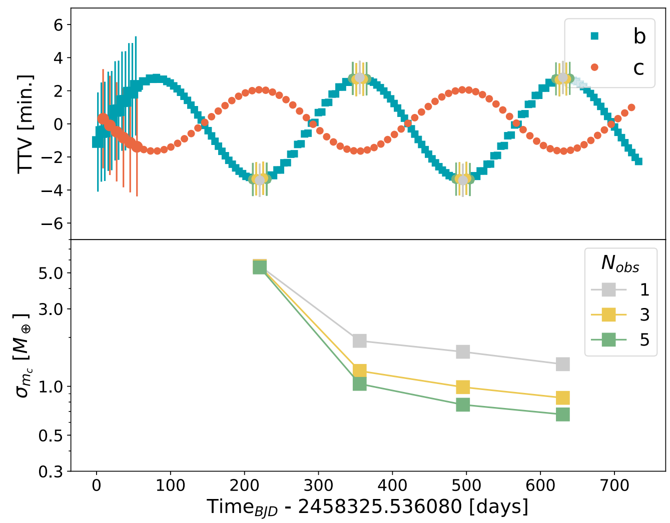

Figure 8. The top panel shows predicted transit times of TOI-125 b (blue) and c (orange) with representative 1σ error bars from the first two *TESS* sectors. The projected TTV signals assume fiducial planet masses of $8.6\,M_\oplus$ and a stellar mass $M_* = 0.87\,M_\odot$. A series of hypothetical follow-up transit observations of planet b with one-minute transit mid-time uncertainties are shown by colored points at the peaks of the TTV signal of planet b. Different color points correspond to follow-up scenarios in which one, three, or five transit observations are obtained at each epoch. The bottom panel shows the expected 1σ uncertainty in the mass of planet c, σ_c, that would be achieved by these follow-up transit observations.

5.2. Dynamical Stability

In the absence of external perturbations, a planet with an eccentric orbit residing close to its host star would generally become tidally circularized on astronomically short timescales (the exact timescale depends on the tidal quality factor of the planet and properties of its host star; see, e.g., Equation (1)). Therefore, significant eccentricities for compact systems often require that the planets be located in regions of resonance (Beaugé et al. 2006) and can result in significant transfer of angular momentum between planets (Kane & Raymond 2014; Antoniadou & Voyatzis 2016). Thus, a dynamical analysis of a proposed orbital solution can be used to validate or potentially revise the allowed architecture for the system. The EXOFASTv2 global model of the TOI-125 multi-planet system cannot exclude a moderately high eccentricity of TOI-125 b ($\sim$0.18), which would be unusual for a planet in a tightly packed, multi-planet system (Kane et al. 2012; Hadden & Lithwick 2014; Van Eylen & Albrecht 2015; Xie et al. 2016). We therefore set out to investigate whether such high eccentricities can be ruled out through dynamical simulations, or if evidence exists that TOI-125 b and TOI-125 c are in resonance.

In the analysis that follows, we consider only the three high-S/N transit signals (TOI-125 b, c, and .03). The candidate USP planet (TOI-125.04), given its small size and orbital period, is effectively dynamically decoupled from the other planets, and if it exists, should not affect our conclusions. TOI-125.05

[51] The total eccentricity of a planet is a combination of its free eccentricity plus a component induced by the gravitational influence of its perturbing companions (see, e.g., Lithwick et al. 2012). The free eccentricity is dissipated in the presence of tidal eccentricity damping, while the forced eccentricity will remain. Because of its short orbital period, the eccentricity damping timescale of planet b is short. Adopting the best-fit stellar mass, planet radius, and orbital period from Table 5, the tidal eccentricity damping timescale for TOI-125 b is given by

$$\left(\frac{1}{e_b}\frac{de_b}{dt}\right)^{-1} = 83\ \mathrm{Myr} \times \left(\frac{Q/k_2}{10^3}\right)\left(\frac{m_b}{10\,M_\oplus}\right), \quad (1)$$

where Q is the planet's tidal quality factor and k_2 its tidal Love number (Goldreich & Soter 1966). The parenthetical terms on the right-hand side are of order unity. With the same assumptions about Q/k_2 for planet c, its nominal eccentricity damping timescale is 1.9 Gyr. Dynamical coupling between b and c should enhance the efficiency with which the eccentricity of planet c is damped, and we thus expect only the forced eccentricity to remain.

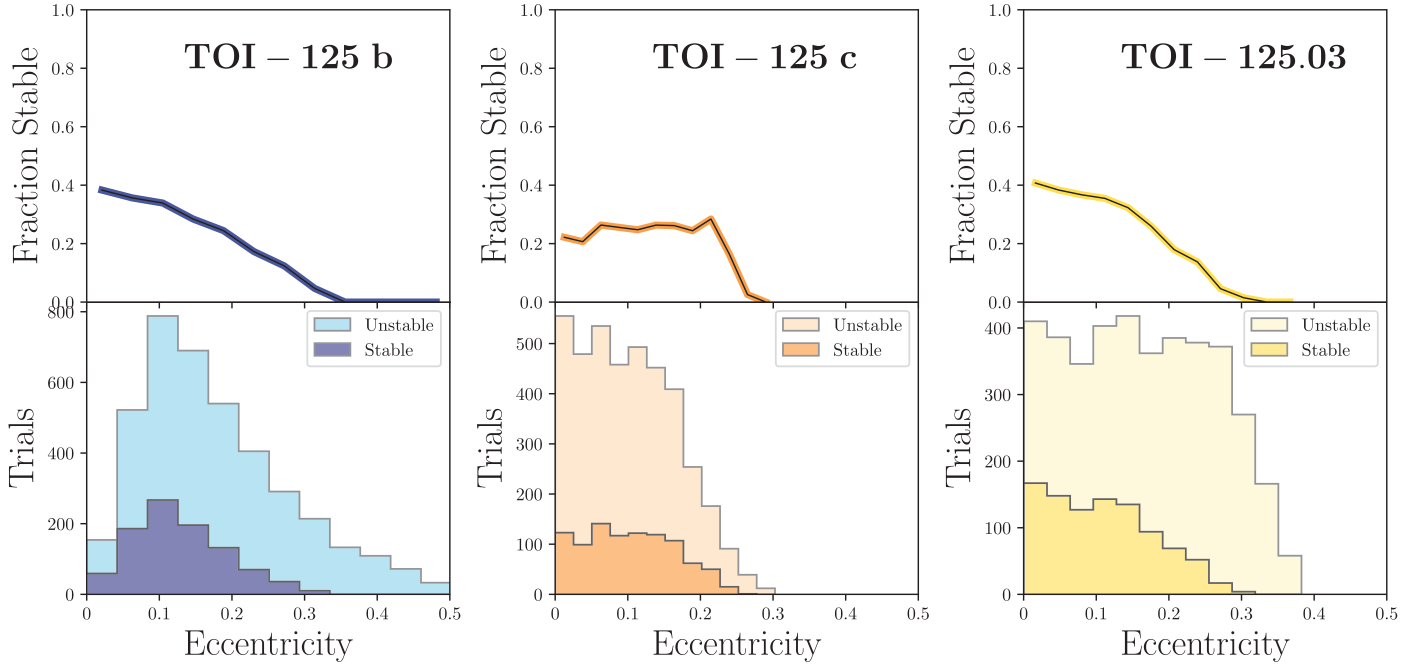

Figure 9. For each planet, the dynamically allowed range of orbital eccentricities, derived from the suite of 1 Myr numerical simulations. (Top panels) For each planet, the fraction of integrations in each planetary eccentricity bin that remains dynamically stable for the entire 1 Myr integration. (Bottom panels) For each planet, stacked histograms showing the stable and unstable trials for each eccentricity. The overall shape of the histograms is determined by the EXOFASTv2 fit results, from which initial simulation parameters were drawn. The results of the simulation used to create this figure are available as a machine-readable table, and the full simulation results are available upon request.

(The data used to create this figure are available.)

would have to be incorporated in a dynamical investigation if it is shown to be real, but given its low S/N, we do not include it in our analysis for now. If follow-up observations show that TOI-125.05 is real, it would reside slightly interior to the 3:2 mean motion commensurability (with a period ratio of ~1.45), close to the regime in which resonant interactions are most relevant.

To evaluate the dynamical stability and orbital evolution of the three planets in the TOI-125 system, we performed 3000 numerical simulations using the *N*-body code `Mercury6` (Chambers 1999), altered to include the effect of general relativistic precession. The simulations were performed using a hybrid symplectic and Bulirsch–Stoer (B-S) integrator with a time-step of 30 minutes for a total integration time of slightly more than 1 million years per integration (which is roughly 80 million orbits of the innermost planet), and energy was conserved to better than one part in 10^9 (for energy changes due to the integrator). For each integration, we drew one link from the EXOFASTv2 transit fit posterior, and assigned planet and star properties equal to those in the chosen posterior link.

These numerical simulations allow us to impose an additional level of constraints beyond those derived from the transit shapes: some planetary eccentricities will lead to dynamical instabilities in the system (which occur when scattering events or orbit crossing leads to physical collisions between planets, the ejection of a planet from the system, or collision of a planet with the central star). The composite eccentricity distributions (stacked stable and unstable) in Figure 9 show the eccentricity draws for our 3000 simulations. The stable subset of each distribution contains those that allow the planets to remain dynamically stable for the entire 1 Myr integration. Not shown is the variation in other orbital elements (also drawn from the EXOFASTv2 posteriors), but the overall trend in stability fraction is shown in the top panels.

Of these 3000 simulations, 32% remained dynamically stable for the entire 1 Myr integration, and Figure 9 shows a higher stability fraction at lower eccentricity values. Dynamical stability considerations thus prefer the lower eccentricity values, and eccentricities above 0.25–0.3 are disallowed for each planet. The conclusion from this analysis is that although the EXOFASTv2 posteriors allow an unusually large range of eccentricities, the true values are likely on the lower ends of these ranges. We find all three orbits to be consistent with circular, but we note that the dynamical analysis shows a preference for a low nonzero eccentricity for TOI-125 b.

5.3. Resonant Behavior and Formation History

The orbital periods of the two planets b and c (4.65437 and 9.1536 days) lie close to the mutual 2:1 commensurability. As a result, it is natural to wonder whether the two planets are trapped in mutual 2:1 MMR (with a period ratio of 1.967). As orbital elements (including semimajor axis) librate while planets reside in resonance, it is possible to reside in resonance even without a perfect 2:1 period ratio (i.e., Batygin & Morbidelli 2013).

However, the majority of planets near but not in orbital resonance reside slightly outside of a resonant configuration. The results of Terquem & Papaloizou (2019, see Figure 9) show that for planets migrating in a disk, it is very easy for the 2:1 resonance to be disrupted when the inner planet enters a disk cavity, as might occur at small orbital radii. The subsequent evolution of the system is more difficult to model, but it is expected that departures from resonance will move toward the outside of resonance in cases where

$$\delta = \frac{P_2}{P_1} - \frac{(q+1)}{q} > -0.04. \quad (2)$$

Here, the resonance considered is the $q + 1$: q first-order resonance. Because the inner two planets in the TOI-125 system have $\delta = -0.033$, they would be expected to fit this trend and reside slightly outside of the 2:1 MMR period ratio; however, these planets instead appear to have a period ratio slightly lower than this value. There are three potential explanations for this:

(1) These planets are currently in true orbital resonance. A system with a similar architecture to TOI-125 is the Gliese-876 system (Marcy et al. 2001; Rivera et al. 2010), which also has two planets close to the 2:1 resonance (Gliese-876 c and b, at ∼30 and ∼60 days), the inner of which exhibits significant (0.2) eccentricity. In the Gliese-876 system, these two planets form a Laplace resonance with a third planet. The nonzero planetary eccentricities are maintained through the resonance. The TOI-125 system also has three high-S/N planets with orbital periods moderately close to 2:1 resonances. An orbital resonance that persisted after the disk dissipated could explain the high eccentricity of the inner planet. While the disk is present, the orbital eccentricity of both planets in the system will be damped. After the disk has dissipated, the eccentricities of the resonant pair is free to grow (and experience secular cycles) due to interactions with other additional planets in the system (in the TOI-125 system, there appear to be several additional planets; furthermore, an increased eccentricity for either planet involved in the resonance may change the resonance width and eventually lead to the disruption of the resonance; Wittenmyer et al. 2012; Malhotra et al. 2018).

Beaugé et al. (2003) present solutions, inspired by Gliese-876, for stable aligned pericenters in the 2:1 resonance. Notably, stable solutions must have non-null eccentricities for the inner planet, and for an inner eccentricity of about 0.3, the outer planet must have a non-null eccentricity as well (for equal-mass planets). The EXOFASTv2 posteriors indicate that TOI-125 c could have a nonzero eccentricity; however, the pericenters are not well enough constrained to determine whether this aligned scenario occurs.

Using our suite of *N*-body simulations, we can evaluate the fraction of fitted posteriors which are consistent with a resonant configuration for planets b and c. Of the 3000 trials considered, 32% are dynamically stable. Of this stable subset, only one began in a true resonance (as defined by a librating resonant angle) and remained so for the entire integration. However, some of the integrations show that the planets can attain and lose a resonant configuration through their natural orbital evolution: in 7% of the dynamically stable integrations, TOI-125 b and c attain a true 2:1 MMR for at least some of the integration (generally for periods around 10^5 yr at a time) but are subsequently disrupted from that resonance. A further 1% attain resonance during the integration and remain stable in that resonance for the entire remaining 1 Myr integration. However, 86% of the dynamically stable integrations never attain a resonant configuration. Barring one single integration that after a scattering interaction attained the 5:3 true resonance, the remaining ∼5% of the stable simulations exhibit (for at least some of the integration, but not a majority) a "nodding" behavior (i.e., Ketchum et al. 2013) in and out of the 2:1 resonance.

From this suite of simulations, it appears that the vast majority of the dynamically stable posteriors are fully nonresonant. However, a true orbital resonance could explain both the eccentricity of the inner planet and the continued stability of the system. The simulations show that this system, if in resonance, is likely characterized by nonconsistent attainment of true resonance.

(2) These planets formed in situ or via inward scattering and do not have resonance in their history. Terquem & Papaloizou (2019) note that only about 15% of systems are consistent with smooth, disk-driven migration, which results in systems with $0 < \delta < 0.04$ (the "outside of resonance" population that is common in the observational sample). If TOI-125 was in resonance while the disk was still present (required if it assembled via disk-driven migration), it should have moved toward positive δ while in resonance and ended with orbits consistent with this population. Its small negative value of δ can be explained if the system did not assemble via smooth migration, is not in resonance, and reached its current proximity to resonance by chance.

(3) These planets formed via disk-driven migration and were in resonance, but are no longer in resonance. As discussed in Adams et al. (2008) and Batygin & Adams (2017), turbulent fluctuations in the disk can destabilize resonances for small planets. These planets are both 2.7 Earth radii, slightly larger than should be possible to turbulently force out of resonance according to Batygin & Adams (2017). However, the 2:1 resonance is rather weak. The resonant angles for this resonance therefore generally have a large libration amplitude, potentially permitting either liberation from true resonance with minor perturbations, or large excursions in orbital element libration. As demonstrated by the numerical simulation, a sizable fraction of the posteriors attain and subsequently lose the 2:1 resonance during the integrations (sometimes multiple times).

6. Discussion

Of the 4723 *Kepler* planets and planet candidates discovered to date,[52] the majority are smaller than Neptune and larger than Earth, and they orbit within a few tenths of an astronomical unit (e.g., Thompson et al. 2018), a class of planet that is not seen in the solar system. The occurrence rates of these short-period super-Earths and mini-Neptunes indicate that they are common byproducts of star formation (e.g., Fressin et al. 2013; Petigura et al. 2013; Dressing & Charbonneau 2015). Their physical and orbital properties therefore hold a wealth of information about the processes governing planet formation and evolution that were previously unconstrained by observation. The ensemble properties of these planets have revealed some of their fundamental characteristics (e.g., Fulton et al. 2017; Berger et al. 2018; Fulton & Petigura 2018), and detailed investigations of individual systems can complement the information gained from population studies.

6.1. Radial-velocity Characterization

The observed bimodality in the radius distribution of *Kepler* planets (e.g., Owen & Wu 2013; Fulton et al. 2017; Zeng et al. 2017), with peaks at ∼1.3 and 2.4 $R_\oplus$ can be reproduced theoretically from the photoevaporation of close-in low-mass

[52] *Kepler* objects of interest reported as confirmed or candidate planets in the NASA Exoplanet Archive on 2018 October 22.

planets, which are stripped to their bare (∼1.3 $R_\oplus$) cores, while more massive planets hold on to their H/He envelopes (e.g., Owen & Wu 2017; Jin & Mordasini 2018). If this were universally true, then the larger of these planets should be more or less the same mass as their smaller counterparts because a H/He envelope will contribute a significant fraction of a planet's radius but very little mass. However, some planets with radii between 2 and 3 $R_\oplus$ appear too dense for this scenario (see, e.g., the recent *TESS* discovery of HD 21749 b; Dragomir et al. 2019). One explanation is that these denser sub-Neptune planets correspond to those in the large-core tail of the distribution. Another explanation is that planet formation proceeds hierarchically, first accreting a rocky core, followed by CNO (e.g., water), and finally H/He, suggesting that planets of ∼2.4 $R_\oplus$ correspond to "water worlds"—planets with a high mean-molecular-weight envelope (Zeng et al. 2017, 2018). However, this alternative would not explain the low-mass large planets that are more consistent with an envelope of H/He. If both modes of planet formation operate, observation can constrain their relative occurrence. Systems like TOI-125, which contains three sub-Neptune planets of similar size and with a range of orbital periods, provide a good opportunity to measure the densities of these planets under controlled conditions. Having been subjected to the same stellar environment, conclusions based on the relative properties of the planets orbiting TOI-125 are less affected by assumptions about stellar evolution and the history of stellar irradiation. Therefore spectroscopic follow-up of TOI-125 may provide insight into planet formation and evolution.

TOI-125 is well suited to precise RV measurements to determine the mass of its planets. The star is a bright ($V = 11.0$; $T = 10.1$) slowly rotating ($v \sin i_\star < 2$ km s^{-1}) late-G dwarf with very little photometric variation ($\sigma_{\rm phot}$). The Chen & Kipping (2017) planetary mass–radius relationship predicts masses of 8.5, 8.6, and 9.5 $M_\oplus$, corresponding to RV semi-amplitudes 3.7, 2.9, and 2.5 m s^{-1}. Given an instrumental precision of ∼1 m s^{-1} for facilities such as HARPS and PFS, we expect that all three planets have detectable RV signals.

We can estimate the time requirements to characterize the TOI-125 system with the HARPS spectrograph using the RVFC tool developed by Cloutier et al. (2018). RV noise sources are estimated as a combination of the instrument noise floor (0.5 m s^{-1}), the photon noise (2.51 m s^{-1} for 30-minute exposures), stellar activity (0.5 m s^{-1} for a worst case $v \sin i_\star$ of 2 km s^{-1}), and the RV rms caused by additional unseen planets (typically 0.4 m s^{-1} in this case). Details of how these noise sources are generated from the known stellar parameters, including Gaussian process (GP) trials to simulate the stellar activity, are given in Cloutier et al. (2018). A complication for this system is its known multiplicity. Additional planets that are perfectly modeled do not impact the characterization of a planet, but because no model is perfect, some additional rms will be present. We use the unseen planet RV rms estimate from RVFC as a zero-order guess at this contribution to the noise budget. We take the longest period planet as the driver of the necessary observations, implicitly assuming that observations sample the orbital phase curve of that and each interior planet well, and that all planets are on circular orbits. Although photon noise dominates for this apparently low-activity star, the effect of stellar activity can be large depending on the rotation period of the star, and in particular whether it is near a harmonic of the planet orbital periods. We present several representative cases, each calculated using the given stellar parameters, estimated planetary masses, and 10 GP trials to estimate stellar activity. To characterize the system with a 5σ detection of the semi-amplitude for the outer planet (TOI-125.03), RVFC predicts 68 ± 9 RV observations for a stellar rotation period of 25 days, rising to 141 ± 37 observations for a difficult case rotation period of 40 days, double the orbital period of candidate .03. For the case of a 20-day stellar rotation period, characterizing candidate .03 becomes untenable, with RVFC predicting 45 ± 5 observations to characterize only planets b and c.

If real, the low S/N events TOI-125.04 and TOI-125.05 may complicate the RV detection of the other three planets, but they are also predicted to have detectable RV signals. With a timescale very different from the other planets and a predicted semi-amplitude of 2.2 m s^{-1}, TOI-125.04 could be detected with a dedicated high-cadence RV campaign, which would ultimately benefit the detection of the outer signals, as it would otherwise enter as an additional source of noise. TOI-125.05 is the candidate with the lowest S/N and is least likely to prove real, but may also produce a detectable RV signal. Its predicted semi-amplitude given its derived size (4.2 $R_\oplus$) is ∼4.8 m s^{-1}. On the other hand, such a large planet is not typically seen in tightly packed systems. We therefore expect that if it is real, the planet is more likely to reside at the smaller end of the fit posteriors (see Figure 4), with an RV signal on the order of 1–2 m s^{-1}.

6.2. *TOI-125 among the* Kepler *Multis*

Nearly 2000 of the 4723 *Kepler* objects of interest (KOIs) reside in multi-planet systems, and their orbital architectures provide clues to their formation and evolution: the typical mutual inclination of short-period systems can be derived from the number of planets per system (e.g., Lissauer et al. 2011b; Fang & Margot 2012; Ballard & Johnson 2016), and from the ratio of transit durations within each system (e.g., Fang & Margot 2012; Fabrycky et al. 2014), and hold information on the dynamical histories of planetary systems; the sizes and orbital spacing of neighboring planets hold information about formation and physical evolution (e.g., Weiss & Marcy 2014); the assembly of planets from planetesimals in the inner region of the protoplanetary disk can be examined through the lens of the present-day properties of short-period planets (e.g., Lee & Chiang 2017).

One striking feature of the population of *Kepler* multi-planet systems is the distribution of period ratios near first-order MMRs. As discussed in Section 5, there is an underdensity of planet pairs just interior to first-order resonances—particularly the 2:1 resonance—and an excess of systems just exterior to resonance. We present an updated histogram of period ratios for *Kepler* systems in Figure 10 (see Steffen et al. 2010; Fabrycky et al. 2014, for a broader discussion of these data), and we note that TOI-125 b and c have a period ratio that falls right in the gap interior to the 2:1 resonance. We have explored possible causes for this in Section 5, and here we compare TOI-125 to the small handful of other systems in or near this gap, shown in the inset of Figure 10.

None of the five other systems interior to but within 2% of 2:1 is quite like TOI-125, which is larger and/or has a shorter period than the others. Kepler-176 d (KOI-520.03) is most similar in size to TOI-125 b and c, but along with *Kepler*-334 (KOI-1909) has a longer period (weeks, rather than days; Rowe et al. 2014). Kepler-271 (KOI-1151) and KOI-4504 have

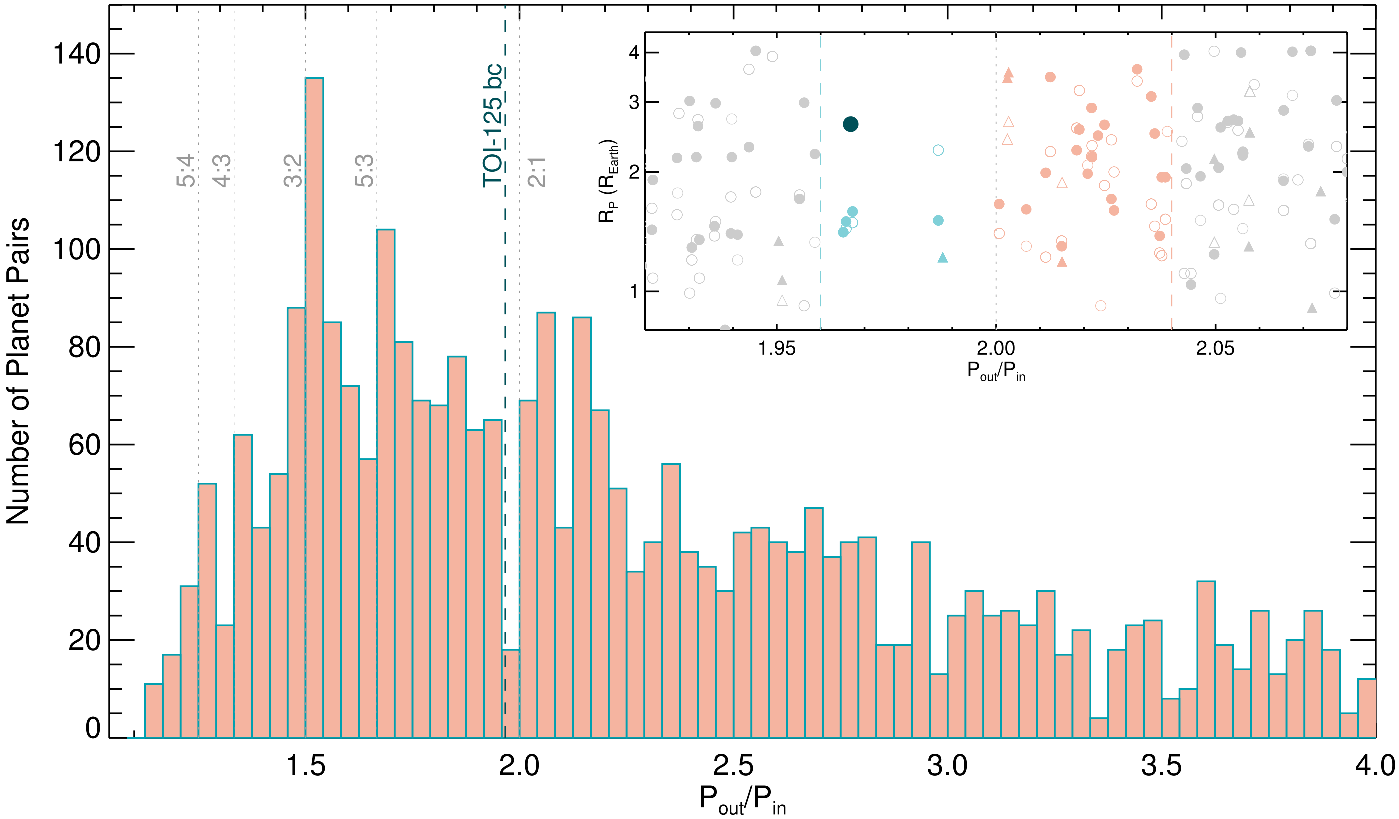

Figure 10. Distribution of period ratios of all pairs of *Kepler* candidates in multi-planet systems, excluding known false positives (orange histogram). Low-order resonances are shown in gray with dotted lines. The period ratio of TOI-125 c and b is indicated by the vertical dashed blue line, and lies in the underpopulated region just short of 2:1. *Inset*: Pairs of radii plotted against their period ratios near the 2:1 MMR. The excess of systems just wide of resonance (orange) and the dearth of systems just shy of resonance (blue) is apparent. Inner planets are shown with open symbols and outer planets with filled symbols. Circles and triangles represent adjacent and non-adjacent planet pairs, respectively. TOI-125 is the larger dark blue circle; b and c lie on top of one another, and are the largest planets in the period ratio gap.

similar periods to TOI-125, but the planets are much smaller. One other system (KOI-1681) has an interesting architecture, with one small planet and one hot Jupiter (similar to WASP-47; Becker et al. 2015), but it also has a nearby stellar companion, a third signal that is likely a false positive, and a fourth signal corresponding to another giant planet candidate. If real, it would be unlike any other system that we know. TOI-125 is thus unusual even within its sparsely populated region of parameter space, and worthy of additional study.

6.3. The Candidate USP Planet TOI-125.04

While TOI-125.04 was only detected with an $S/N \sim 5.2$, the presence of three high-S/N transit signals in the system makes it more likely that the signal is real compared to an isolated signal of similar strength. Moreover, the architecture of the TOI-125 planets would match that of other known USP systems, both in semimajor axis and in mutual inclination. Dai et al. (2018) find that *Kepler* and *K2* planets in multi-planet systems tend to exhibit high mutual inclinations when the innermost planet has a small semimajor axis ($a/R_* < 5$), and that of these USP planets, the systems with the highest mutual inclinations also have high period ratios (see, e.g., K2-266, with an extreme mutual inclination of $\sim 12°$; Rodriguez et al. 2018b). TOI-125.04 orbits at ($a/R_* \sim 3.1$) and with a projected mutual inclination of $\sim 16°$. The period ratio between TOI-125 b and TOI-125.04 is 8.8, similar to the other such misaligned USP planets. TOI-125.04 would be the USP planet with the highest known mutual inclination, but as discussed above, TOI-125 b is larger than most inner planets in packed systems. We speculate that in the framework suggested by Dai et al. (2018), one would expect the interaction between the two planets that leads to the inclined USP planet to produce a more extreme outcome when the adjacent planet is more massive than usual.

6.4. Dynamical Results

The EXOFASTv2 transit fit allowed a relatively wide range in eccentricities for TOI-125 b, c, and d, but the highest of the allowed values can be excluded due to dynamical stability constraints. Of the entire EXOFASTv2 posteriors, approximately 32% of draws result in integrations that remain dynamically stable for 1 Myr. Preferentially, the stable subsets are those with lower eccentricities: eccentricities above 0.25–0.3 are disallowed for each planet (see Section 5.2).

Using the results of the numerical simulations to gain information on the resonant behavior, we obtain a largely nonresonant picture of the posteriors. Of the stable subset of integrations, roughly 86% exhibited nearly exclusively nonresonant behavior for planets b and c. In these cases, the median period ratio libration has a (min-to-max) amplitude of $\Delta\delta \approx 0.01$, surrounding a median δ value of $\delta \approx -0.032$ (compared to the measured current value of $\delta \approx -0.033$). From these simulations, it is reasonable to assume that the observed three-planet system can remain dynamically stable in the observed orbits for a relatively large fraction of the EXOFASTv2 posteriors. For the ∼12% of integrations that reside in or nod in/out of the 2:1 resonance for some or all of of the 1 Myr, the size of $\Delta\delta$ depends on the libration width of the resonant angle. For nodding, this value is as high as ≈0.08, around a median δ value of $\delta \approx 0.001$. In true resonance, the typical $\Delta\delta$ values range between 0.02 and 0.04, and the median δ value becomes closer to $\delta \approx 0$. It is possible that TOI-125 b and c previously resided in 2:1 resonance and naturally lost the resonance at some point, becoming trapped in a dynamically stable but nonresonant orbit Although the errors on the currently measured orbit are too large to conclusively determine the current resonance behavior of TOI-125 b and c, the simulations suggest that they are most likely not in resonance at present, but have eccentricities near the lower end of the measured posteriors.

7. Summary

In this paper, we have presented the *TESS* discovery of the TOI-125 multi-planet system, and we fit a global model to the *TESS* data, spectroscopic stellar parameters, literature photometry, and the *Gaia* parallax in conjunction with stellar models to characterize the planet candidates. We then statistically validated the planetary nature of TOI-125 b and c using `vespa` with the aid of archival imaging and our photometric, spectroscopic, and high-resolution imaging observations. We demonstrated that the system is likely amenable to mass determination via both TTV and precise RV follow-up, and that the planets are worthy of such additional study. The three strongest transit signals are caused by planets with radii 2.8–2.9 $R_\oplus$, a class of planet that is not seen in the solar system but is abundant in the galaxy. These planets have been proposed as the progenitors (via photoevaporation) of the terrestrial planets that are commonly found in short periods around nearby stars, and studying three of them in the controlled environment of the same host star can help illuminate the formation and evolution processes at play. The candidate terrestrial USP planet, with an orbital period shorter than 13 hr and a mutual inclination of 16° with the other planets, is an extreme example of the trend toward such architectures in other known USP planets in multiple systems, and may be the end result of dynamical interaction with its much larger sub-Neptune neighbors. Finally, the period ratio between planets b and c is very near but just interior to a 2:1 commensurability, which is quite unusual compared to known *Kepler* systems. While one possible explanation is that the system is in—and librating about— 2:1 resonance, our dynamical analysis suggests that it is unlikely that the system is currently in true resonance. The discovery of the TOI-125 system demonstrates that *TESS* continues in its early days to deliver on its promise to identify rare systems of small planets amenable to follow-up observations and detailed characterization.

J.C.B. is supported by the NSF Graduate Research Fellowship grant No. DGE 1256260 and by the Leinweber Center for Theoretical Physics. Work performed by J.E.R. was supported by the Harvard Future Faculty Leaders Postdoctoral fellowship. D.J.A. gratefully acknowledges support from the STFC via an Ernest Rutherford Fellowship (ST/R00384X/1). A.V.'s contribution to this work was performed under contract with the California Institute of Technology (Caltech)/Jet Propulsion Laboratory (JPL) funded by NASA through the Sagan Fellowship Program executed by the NASA Exoplanet Science Institute. Work by J.N.W. was supported by the Heising-Simons Foundation. D.D. acknowledges support for this work provided by NASA through Hubble Fellowship grant *HST*-HF2-51372.001-A awarded by the Space Telescope Science Institute, which is operated by the Association of Universities for Research in Astronomy, Inc., for NASA, under contract NAS5-26555. I.J.M.C. acknowledges support from the NSF through grant AST-1824644. A.G. is supported by the Ida M. Green Fellowship. M.T. is supported by MEXT/JSPS KAKENHI grant Nos. 18H05442, 15H02063, and 22000005. This work is partly supported by JSPS KAKENHI grant Nos. JP15H02063, JP18H01265, JP18H05439, JP18H05442, and JST PRESTO grant No. JPMJPR1775. We acknowledge the support provided by the Polish National Science Center through grants 2016/21/B/ST9/01613 and 2017/27/B/ST9/02727.

We thank Zach Hartman and Dan Nusdeo for help with the Gemini-South observations. We thank Akihiko Fukui, Nobuhiko Kusakabe, Kumiko Morihana, Tetsuya Nagata, Takahiro Nagayama, Taku Nishiumi, and the staff of SAAO for their kind support for IRSF SIRIUS observations and analyses.

Funding for the *TESS* mission is provided by NASA's Science Mission directorate. We acknowledge the use of public *TESS* Alert data from pipelines at the *TESS* Science Office and at the *TESS* Science Processing Operations Center. This paper includes data collected by the *TESS* mission, which are publicly available from the Mikulski Archive for Space Telescopes (MAST).

This work used the Extreme Science and Engineering Discovery Environment (XSEDE), which is supported by National Science Foundation grant number ACI-1053575. This research was done using resources provided by the Open Science Grid, which is supported by the National Science Foundation and the U.S. Department of Energy's Office of Science, through allocation TG-AST150033.

The Swiss Euler telescope is supported by the Swiss National Science Foundation. This paper includes observations obtained under ESO/VLT program 0102.C-0503(A), and Gemini program GS-2018B-LP-101. Gemini Observatory is operated by the Association of Universities for Research in Astronomy, Inc., under a cooperative agreement with the NSF on behalf of the Gemini partnership: the National Science Foundation (United States), National Research Council (Canada), CONICYT (Chile), Ministerio de Ciencia, Tecnología e Innovación Productiva (Argentina), Ministério da Ciência, Tecnologia e Inovação (Brazil), and Korea Astronomy and Space Science Institute (Republic of Korea). This work makes use of observations from the LCOGT network. The IRSF project is a collaboration between Nagoya University and the South African Astronomical Observatory (SAAO) supported by the Grants-in-Aid for Scientific Research on Priority Areas (A) (Nos. 10147207 and 10147214) and Optical & Near-Infrared Astronomy Inter-University Cooperation Program, from the Ministry of Education, Culture, Sports, Science and Technology (MEXT) of Japan and the National Research Foundation (NRF) of South Africa. Based in part on data collected with *Solaris* network of telescopes of the Nicolaus Copernicus Astronomical Center of the Polish Academy of Sciences. The research leading to these results has received funding from the European Research Council under the

European Union's Seventh Framework Programme (FP/2007-2013) ERC Grant Agreement 336480, from the ARC grant for Concerted Research Actions, financed by the Wallonia-Brussels Federation, and from a research grant from the Balzan Prize Foundation. TRAPPIST is funded by the Belgian Fund for Scientific Research (Fond National de la Recherche Scientifique, FNRS) under the grant FRFC 2.5.594.09.F, with the participation of the Swiss National Science Fundation (SNF). M.G. and E.J. are FNRS Senior Research Associates.

This work has made use of data from the European Space Agency (ESA) mission *Gaia* (https://www.cosmos.esa.int/gaia), processed by the *Gaia* Data Processing and Analysis Consortium (DPAC, https://www.cosmos.esa.int/web/gaia/dpac/consortium). Funding for the DPAC has been provided by national institutions, in particular the institutions participating in the *Gaia* Multilateral Agreement. This research has made use of NASA's Astrophysics Data System. This research has made use of the VizieR catalog access tool, CDS, Strasbourg, France. The original description of the VizieR service was published in A&AS 143, 23. This research has made use of the SIMBAD database, operated at CDS, Strasbourg, France. This research has made use of the NASA Exoplanet Archive and the Exoplanet Follow-up Observation Program website, which are operated by the California Institute of Technology, under contract with the National Aeronautics and Space Administration under the Exoplanet Exploration Program.

Facilities: TESS, Euler1.2m (CORALIE), Gemini:South (DSSI), SOAR (HRCam), VLT:Antu (NACO), IRSF, LCOGT, SSO:1m, TRAPPIST.

Software: `EXOFASTv2` (Eastman et al. 2013; Eastman 2017), `vespa` (Morton 2015), `Mercury6` (Chambers 1999), `AstroImageJ` (Collins et al. 2017).

ORCID iDs

Samuel N. Quinn https://orcid.org/0000-0002-8964-8377
Juliette C. Becker https://orcid.org/0000-0002-7733-4522
Joseph E. Rodriguez https://orcid.org/0000-0001-8812-0565
Sam Hadden https://orcid.org/0000-0002-1032-0783
Chelsea X. Huang https://orcid.org/0000-0003-0918-7484
Timothy D. Morton https://orcid.org/0000-0002-8537-5711
Fred C. Adams https://orcid.org/0000-0002-8167-1767
David Armstrong https://orcid.org/0000-0002-5080-4117
Jason D. Eastman https://orcid.org/0000-0003-3773-5142
Jonathan Horner https://orcid.org/0000-0002-1160-7970
Stephen R. Kane https://orcid.org/0000-0002-7084-0529
Joseph D. Twicken https://orcid.org/0000-0002-6778-7552
Andrew Vanderburg https://orcid.org/0000-0001-7246-5438
Rob Wittenmyer https://orcid.org/0000-0001-9957-9304
Roland K. Vanderspek https://orcid.org/0000-0001-6763-6562
David W. Latham https://orcid.org/0000-0001-9911-7388
Joshua N. Winn https://orcid.org/0000-0002-4265-047X
Jon M. Jenkins https://orcid.org/0000-0002-4715-9460
Eric Agol https://orcid.org/0000-0002-0802-9145
L. G. Bouma https://orcid.org/0000-0002-0514-5538
David Charbonneau https://orcid.org/0000-0002-9003-484X
Jessie L. Christiansen https://orcid.org/0000-0002-8035-4778
Karen A. Collins https://orcid.org/0000-0001-6588-9574
Tansu Daylan https://orcid.org/0000-0002-6939-9211
Jason Dittmann https://orcid.org/0000-0001-7730-2240
Diana Dragomir https://orcid.org/0000-0003-2313-467X
Michael Gillon https://orcid.org/0000-0003-1462-7739
Ana Glidden https://orcid.org/0000-0002-5322-2315
Krzysztof G. Hełminiak https://orcid.org/0000-0002-7650-3603
Elliott P. Horch https://orcid.org/0000-0003-2159-1463
Steve B. Howell https://orcid.org/0000-0002-2532-2853
Eric L. N. Jensen https://orcid.org/0000-0002-4625-7333
Nicholas Law https://orcid.org/0000-0001-9380-6457
Andrew W. Mann https://orcid.org/0000-0003-3654-1602
Rachel A. Matson https://orcid.org/0000-0001-7233-7508
Norio Narita https://orcid.org/0000-0001-8511-2981
Francisco J. Pozuelos https://orcid.org/0000-0003-1572-7707
Joshua E. Schlieder https://orcid.org/0000-0001-5347-7062
Avi Shporer https://orcid.org/0000-0002-1836-3120
Keivan G. Stassun https://orcid.org/0000-0002-3481-9052
Motohide Tamura https://orcid.org/0000-0002-6510-0681
Carl Ziegler https://orcid.org/0000-0002-0619-7639

References

Adams, F. C., Laughlin, G., & Bloch, A. M. 2008, ApJ, 683, 1117
Agol, E., Steffen, J., Sari, R., & Clarkson, W. 2005, MNRAS, 359, 567
Antoniadou, K. I., & Voyatzis, G. 2016, MNRAS, 461, 3822
Ballard, S., & Johnson, J. A. 2016, ApJ, 816, 66
Barclay, T., Pepper, J., & Quintana, E. V. 2018, ApJS, 239, 2
Batygin, K., & Adams, F. C. 2017, AJ, 153, 120
Batygin, K., & Morbidelli, A. 2013, AJ, 145, 1
Beaugé, C., Ferraz-Mello, S., & Michtchenko, T. A. 2003, ApJ, 593, 1124
Beaugé, C., Michtchenko, T. A., & Ferraz-Mello, S. 2006, MNRAS, 365, 1160
Becker, J. C., Vanderburg, A., Adams, F. C., Rappaport, S. A., & Schwengeler, H. M. 2015, ApJL, 812, L18
Berger, T. A., Huber, D., Gaidos, E., & van Saders, J. L. 2018, ApJ, 866, 99
Borucki, W. J., Koch, D., Basri, G., et al. 2010, Sci, 327, 977
Buchhave, L. A., Latham, D. W., Carter, J. A., et al. 2011, ApJS, 197, 3
Carter, J. A., Yee, J. C., Eastman, J., Gaudi, B. S., & Winn, J. N. 2008, ApJ, 689, 499
Chambers, J. E. 1999, MNRAS, 304, 793
Chen, J., & Kipping, D. 2017, ApJ, 834, 17
Choi, J., Dotter, A., Conroy, C., et al. 2016, ApJ, 823, 102
Ciardi, D. R., Beichman, C. A., Horch, E. P., & Howell, S. B. 2015, ApJ, 805, 16
Claret, A. 2017, A&A, 600, A30
Cloutier, R., Doyon, R., Bouchy, F., & Hébrard, G. 2018, AJ, 156, 82
Collins, K. A., Kielkopf, J. F., Stassun, K. G., & Hessman, F. V. 2017, AJ, 153, 77
Cutri, R. M., Skrutskie, M. F., van Dyk, S., et al. 2003, yCat, 2246, 0
Cutri, R. M., et al. 2014, yCat, 2328, 0
Dai, F., Masuda, K., & Winn, J. N. 2018, ApJL, 864, L38
Delrez, L., Gillon, M., Queloz, D., et al. 2018, Proc. SPIE, 10700, 107001I
Dotter, A. 2016, ApJS, 222, 8
Dragomir, D., Teske, J., Gunther, M. N., et al. 2019, ApJL, 875, L7
Dressing, C. D., & Charbonneau, D. 2015, ApJ, 807, 45
Eastman, J. 2017, EXOFASTv2: Generalized publication-quality exoplanet modeling code, Astrophysics Source Code Library, ascl:1710.003
Eastman, J., Gaudi, B. S., & Agol, E. 2013, PASP, 125, 83
Fabrycky, D. C., Lissauer, J. J., Ragozzine, D., et al. 2014, ApJ, 790, 146
Fang, J., & Margot, J.-L. 2012, ApJ, 761, 92
Ford, E. B. 2006, ApJ, 642, 505
Fressin, F., Torres, G., Charbonneau, D., et al. 2013, ApJ, 766, 81
Fulton, B. J., & Petigura, E. A. 2018, AJ, 156, 264
Fulton, B. J., Petigura, E. A., Howard, A. W., et al. 2017, AJ, 154, 109
Gaia Collaboration, Brown, A. G. A., Vallenari, A., et al. 2016, A&A, 595, A2
Gaia Collaboration, Brown, A. G. A., Vallenari, A., et al. 2018, A&A, 616, A1
Gandolfi, D., Barragán, O., Livingston, J. H., et al. 2018, A&A, 619, L10
Goldreich, P., & Soter, S. 1966, Icar, 5, 375
Hadden, S., Barclay, T., Payne, M. J., & Holman, M. J. 2019, AJ, 158, 146
Hadden, S., & Lithwick, Y. 2014, ApJ, 787, 80

Henden, A. A., Templeton, M., Terrell, D., et al. 2016, yCat, 2336
Høg, E., Fabricius, C., Makarov, V. V., et al. 2000, A&A, 355, L27
Holman, M. J., & Murray, N. W. 2005, Sci, 307, 1288
Horch, E. P., Howell, S. B., Everett, M. E., & Ciardi, D. R. 2012, AJ, 144, 165
Horch, E. P., Veillette, D. R., Baena Gallé, R., et al. 2009, AJ, 137, 5057
Howell, S. B., Sobeck, C., Haas, M., et al. 2014, PASP, 126, 398
Huang, C. X., Burt, J., Vanderburg, A., et al. 2018a, ApJL, 868, L39
Huang, C. X., Shporer, A., Dragomir, D., et al. 2018b, arXiv:1807.11129
Jehin, E., Gillon, M., Queloz, D., et al. 2011, Msngr, 145, 2
Jenkins, J. M., Caldwell, D. A., Chandrasekaran, H., et al. 2010, ApJL, 713, L87
Jenkins, J. M., Twicken, J. D., Batalha, N. M., et al. 2015, AJ, 150, 56
Jenkins, J. M., Twicken, J. D., McCauliff, S., et al. 2016, Proc. SPIE, 9913, 99133E
Jin, S., & Mordasini, C. 2018, ApJ, 853, 163
Kane, S. R., Ciardi, D. R., Gelino, D. M., & von Braun, K. 2012, MNRAS, 425, 757
Kane, S. R., & Raymond, S. N. 2014, ApJ, 784, 104
Ketchum, J. A., Adams, F. C., & Bloch, A. M. 2013, ApJ, 762, 71
Kraus, A. L., Ireland, M. J., Huber, D., Mann, A. W., & Dupuy, T. J. 2016, AJ, 152, 8
Latham, D. W., Rowe, J. F., Quinn, S. N., et al. 2011, ApJL, 732, L24
Lee, E. J., & Chiang, E. 2017, ApJ, 842, 40
Lenzen, R., Hofmann, R., Bizenberger, P., & Tusche, A. 1998, Proc. SPIE, 3354, 606
Lissauer, J. J., Fabrycky, D. C., Ford, E. B., et al. 2011a, Natur, 470, 53
Lissauer, J. J., Marcy, G. W., Rowe, J. F., et al. 2012, ApJ, 750, 112
Lissauer, J. J., Ragozzine, D., Fabrycky, D. C., et al. 2011b, ApJS, 197, 8
Lithwick, Y., Xie, J., & Wu, Y. 2012, ApJ, 761, 122
Malhotra, R., Lan, L., Volk, K., & Wang, X. 2018, AJ, 156, 55
Marcy, G. W., Butler, R. P., Fischer, D., et al. 2001, ApJ, 556, 296
Matson, R. A., Howell, S. B., & Ciardi, D. 2019, AJ, 157, 211
Morton, T. D. 2015, VESPA: False positive probabilities calculator, Astrophysics Source Code Library, ascl:1503.011
Owen, J. E., & Wu, Y. 2013, ApJ, 775, 105
Owen, J. E., & Wu, Y. 2017, ApJ, 847, 29
Paxton, B., Bildsten, L., Dotter, A., et al. 2011, ApJS, 192, 3
Paxton, B., Cantiello, M., Arras, P., et al. 2013, ApJS, 208, 4
Paxton, B., Marchant, P., Schwab, J., et al. 2015, ApJS, 220, 15
Pepe, F., Bouchy, F., Mayor, M., & Udry, S. 2018, in Handbook of Exoplanets, ed. H. Deeg & J. Belmonte (Berlin: Springer), 190
Pepe, F., Mayor, M., Galland, F., et al. 2002, A&A, 388, 632
Petigura, E. A., Howard, A. W., & Marcy, G. W. 2013, PNAS, 110, 19273
Petigura, E. A., Schlieder, J. E., Crossfield, I. J. M., et al. 2015, ApJ, 811, 102
Price, E. M., & Rogers, L. A. 2014, ApJ, 794, 92
Queloz, D., Mayor, M., Weber, L., et al. 2000, A&A, 354, 99
Ricker, G. R., Winn, J. N., Vanderspek, R., et al. 2015, JATIS, 1, 014003
Rivera, E. J., Laughlin, G., Butler, R. P., et al. 2010, ApJ, 719, 890
Rodriguez, J. E., Becker, J. C., Eastman, J. D., et al. 2018b, AJ, 156, 245
Rodriguez, J. E., Vanderburg, A., Eastman, J. D., et al. 2018a, AJ, 155, 72
Rousset, G., Lacombe, F., Puget, P., et al. 1998, Proc. SPIE, 3353, 508
Rowe, J. F., Bryson, S. T., Marcy, G. W., et al. 2014, ApJ, 784, 45
Schlegel, D. J., Finkbeiner, D. P., & Davis, M. 1998, ApJ, 500, 525
Stassun, K. G., Oelkers, R. J., Pepper, J., et al. 2018, AJ, 156, 102
Steffen, J. H., Batalha, N. M., Borucki, W. J., et al. 2010, ApJ, 725, 1226
Stumpe, M. C., Smith, J. C., Van Cleve, J. E., et al. 2012, PASP, 124, 985
Sullivan, P. W., Winn, J. N., Berta-Thompson, Z. K., et al. 2015, ApJ, 809, 77
Terquem, C., & Papaloizou, J. C. B. 2019, MNRAS, 482, 530
Thompson, S. E., Coughlin, J. L., Hoffman, K., et al. 2018, ApJS, 235, 38
Tokovinin, A. 2018, PASP, 130, 035002
Van Eylen, V., & Albrecht, S. 2015, ApJ, 808, 126
Vanderburg, A., Latham, D. W., Buchhave, L. A., et al. 2016, ApJS, 222, 14
Vanderspek, R., Huang, C. X., Vanderburg, A., et al. 2019, ApJL, 871, L24
Weiss, L. M., & Marcy, G. W. 2014, ApJL, 783, L6
Wittenmyer, R. A., Horner, J., & Tinney, C. G. 2012, ApJ, 761, 165
Xie, J.-W., Dong, S., Zhu, Z., et al. 2016, PNAS, 113, 11431
Yee, S. W., Petigura, E. A., & von Braun, K. 2017, ApJ, 836, 77
Zeng, L., Jacobsen, S. B., Hyung, E., et al. 2017, in LPSC, 48, 1576
Zeng, L., Jacobsen, S. B., Sasselov, D. D., & Vanderburg, A. 2018, MNRAS, 479, 5567
Ziegler, C., Law, N. M., Baranec, C., et al. 2018a, AJ, 156, 259
Ziegler, C., Law, N. M., Baranec, C., et al. 2018b, AJ, 155, 161